Computation and Simulation in Mechanical Sciences (CSMech)

# Surface stress size dependency in postbuckling characteristics of nanoshells under lateral and hydrostatic pressures

S. Sahmani

ORIGINAL PAPER

Open Access

**Volume: 01**

**Issue: 01**

**Winter 2018**

**Page: 53-70**

**ISSN:**

**eISSN:**

**www.csmech.iaubanz.ac.ir**

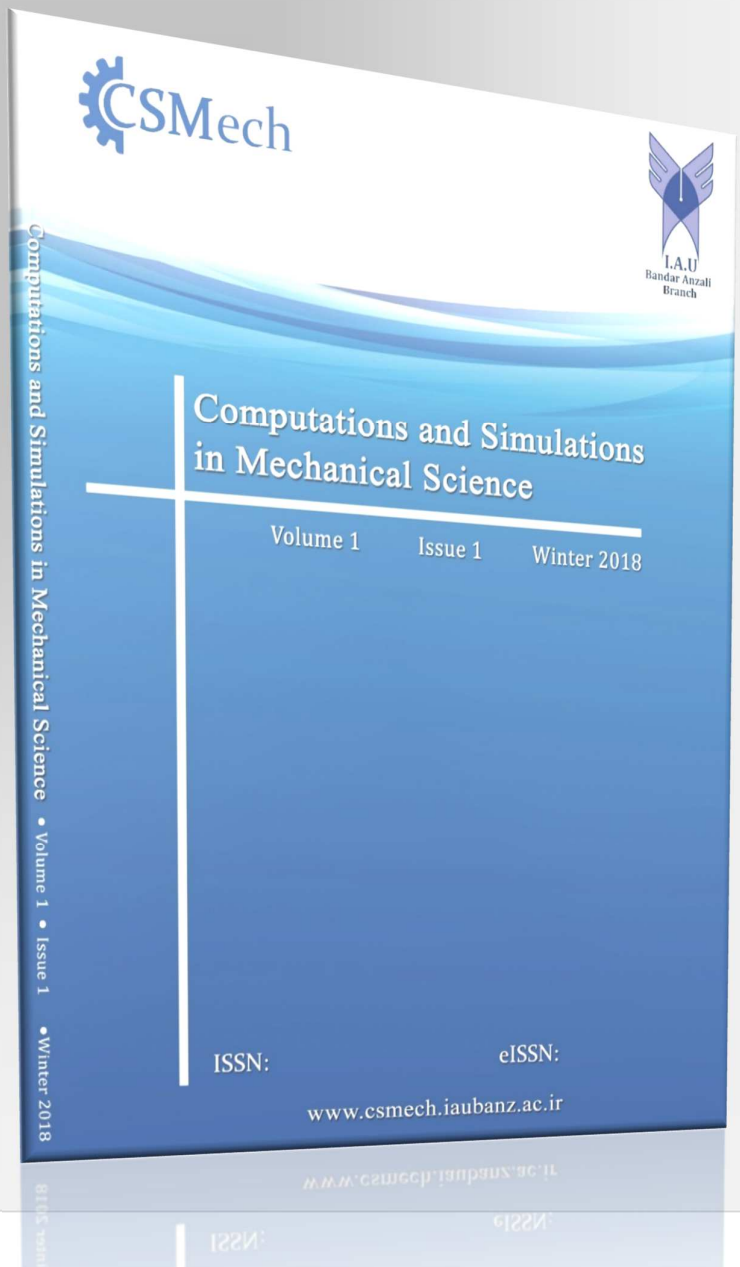

CSMech. 01(01), 53-70, (2018)

Computations and Simulations in Mechanical Science

ORIGINAL PAPER

CSMech

www.csmech.iaubanz.ac.ir

I.A.U Bandar Anzali Branch

# Surface stress size dependency in postbuckling characteristics of nanoshells under lateral and hydrostatic pressures

S. Sahmani [a,*]

[a] *Department of Mechanical Engineering, Amirkabir University of Technology, P.O. Box* 15875-4413*, Tehran, Iran*

## Abstract

The prime aim of the current study is to predict the nonlinear buckling and postbuckling behavior of cylindrical nanoshells subjected to two different radial compressive loads including lateral pressure and hydrostatic pressure with the presence of surface stress effects. The Gurtin-Murdoch elasticity theory in conjunction with von Karman geometrical nonlinearity relations is implemented into the classical shell theory to develop size-dependent shell model incorporating the effects of surface stress. Consequently, to satisfy the balance conditions on the free surfaces of nanoshell, a linear variation through the thickness is considered for the normal stress component of the bulk in such a way that it diminishes on mid-plane and is equal to shear surface stress components on the free surfaces. Afterwards, a boundary layer theory is employed which considers both nonlinear prebuckling deformations and large deflections in the postbuckling domain. Finally, a singular perturbation technique is utilized to obtain the critical buckling loads and the postbuckling equilibrium paths of nanoshells including surface stress effects and corresponding to both loading cases. It is revealed that surface stress effect has a more significant influence on the postbuckling behavior of nanoshells with lower thicknesses. Also, it is found that this pattern is some deal more considerable for the hydrostatic pressure loading case compared to the lateral pressure one.

**Article history**

Received: 2017-12-25
Revised: 2018-01-16
Accepted: 2018-02-29

**Keywords**

Nanomechanics
Size effects
Nonlinear buckling
Cylindrical shells
Boundary layer theory

## 1. Introduction

A new era in science has been opened by development of nanoscience and nanotechnology that leads to an increasing impetus for nanoscale materials in order to design complex nanostructures. The structures at nanoscale such as nanowires, nanobeams and nanoshells can be identified as the consequences of molecular manipulation that are recognized as the essential parts of several nanosystems and nanodevices. Because of the light weight but high stiffness of these submicron scale structures, they can be an ideal choice to be applied in space.

Due to difficulties encountered in the experimental methods to predict the responses of nanostructures under different loading conditions as the size of physical systems is scaled down into the nanoscale, theoretical analyses have gained more attention. Therefore, the classical continuum mechanics has been widely used to investigate various characteristics of nanostructures [1-5]. However, the length scales associated with materials of nanostructures are too small for the applicability of the classical continuum models calls to question. Indeed, size effect is intrinsic in analysis of structures at nanoscale. As a result, several non-classical continuum elasticity theories have been proposed and used to predict size-dependent mechanical behaviors of nanostructures [6-20].

One of such molecular effects is the effects of surface free energy which has been clearly indicated and explained [21, 22]. Due to the different environment conditions, atoms at or near a free surface have different equilibrium requirements compared to the atoms in the bulk of the material. This difference causes an excess surface energy since a surface can be interpreted as a layer to which certain energy is attached [23].

*Corresponding author: S. Sahmani
E-mail address: sasahmani@gmail.com

## List of symbols

| | |
|---|---|
| $A_{ij}, D_{ij} - a_{ij}, d_{ij}$ | Stiffness parameters – Dimensionless stiffness parameters |
| $E$ | Elastic modulus |
| $F - f$ | Airy stress function – Dimensionless airy stress function |
| $h$ | Nanoshell thickness |
| $L$ | Nanoshell length |
| $m$ | Axial half-wave number |
| $M_{ij}$ | Moment stress resultants |
| $n$ | Circumferential wave number |
| $N_{ij}$ | Force stress resultants |
| $q$ | External pressure |
| $R$ | Nanoshell radius |
| $x, y, z - X, Y, Z$ | Coordinate components – Dimensionless coordinate components |
| $\beta$ | Dimensionless parameter |
| $\Gamma$ | Dimensionless parameter related to boundary layer solution |
| $\delta$ | Kronecker delta |
| $\varepsilon_{ij}$ | Strain components |
| $\zeta$ | Dimensionless parameter related to boundary layer |
| $\eta$ | Dimensionless parameter |
| $\kappa_{ij}$ | Curvature components |
| $\lambda - \lambda_s$ | Lame constant – Surface Lame constant |
| $\mu - \mu_s$ | Lame constant – Surface Lame constant |
| $\nu$ | Poisson's ratio |
| $\xi$ | Dimensionless parameter related to boundary layer |
| $\Pi$ | Strain energy |
| $\sigma_{ij} - \sigma_{ij}^s$ | Stress components – Surface stress components |
| $\tau_{ij}$ | Shear stress components |
| $\tau_s$ | Surface residual stress |
| $\gamma_{ij}$ | Shear strain components |
| $\Psi_i - \psi_i$ | Rotation components – Dimensionless rotation components |
| $\mathcal{A}_{ij}, \mathcal{B}_{ij}$ | Dimensionless constants related to displacements |
| $\mathcal{P}_q$ | Dimensionless radial load |
| $\delta_q$ | Dimensionless shortening |
| $\epsilon$ | Perturbation parameter |
| $\mathcal{L}_i$ | Derivative operators |
| $\mathcal{S}_i$ | Dimensionless parameters related to perturbation solution |
| $\Delta_x$ | Shortening |

Gurtin and Murdoch [24, 25] developed a theoretical framework based on the continuum mechanics including surface stress effect which has an excellent capability to incorporate the surface stress effect into the mechanical responses of nanostructures. Based on this type of continuum elasticity theory, the surface is simulated as a mathematical layer of zero thickness with different material properties derived from the underlying bulk material. A variety of problems at nanoscale have been analyzed on the basis of Gurtin-Murdoch elasticity theory. Herein, some of the investigations carried out about the effect of surface energy on the mechanical behaviors of nanostructures are cited.

Wang and Feng [26] and Abbasion et al. [27] investigated the free vibration response of microscale beam including surface effects on the basis of Euler-Bernoulli and Timoshenko beam theories, respectively. Tian and Rajapakse [28] implemented the surface elasticity theory to examine the surface-interface stress effects on the elastic field of an

isotropic matrix with a nanoscale elliptical inhomogeneity.

Lü et al. [29] presented a generalized refined theory incorporating the influence of surface stress for functionally graded films based on Gurtin-Murdoch elasticity theory. Zhao and Rajapakse [30] proposed the axisymmetric solutions for an elastic layer subjected to surface loading incorporating the effects of surface energy. Fu et al. [31] studied the influences of surface energy on the free vibration and buckling behavior of nanobeams in both linear and nonlinear regimes using Galerkin technique. Ansari and Sahmani [32] analyzed the bending and buckling behaviors of nanobeams including the effect of surface stress corresponding to different beam theories. Ansari and Sahmani [33] also predicted the free vibration of rectangular nanoplates based on surface elasticity theory. They implemented Gurtin-Murdoch elasticity theory into the classical and first-order shear deformation plate theories. Ansari et al. [34, 35] predicted the postbuckling characteristics of Euler-Bernoulli and Timoshenko nanobeams, respectively, with the presence of the surface stress effects. On the basis of Gurtin-Murdoch elasticity theory, Ansari et al. [36] investigated the pull-in instability of hydrostatically and electrostatically actuated circular nanoplates including surface stress effect. Sahmani et al. [37] predicted the free vibration response of postbuckled third-order shear deformable nanobeams based on surface elasticity theory. Sahmani et al. [38] used Gurtin-Murdoch elasticity theory to develop a non-classical beam model to study the nonlinear forced vibrations of nanobeams including surface effects. Sahmani et al. [39] examined the free vibration of postbuckled circular higher-order shear deformable nanoplates incorporating the effect of surface free energy. Cheng and Chen [40] employed surface elasticity theory to obtain the size-dependent resonance frequency and buckling load of rectangular nanoplates. Sahmani et al. [41] studied the free vibration characteristics of postbuckled functionally graded third-order shear deformable nanobeams using surface elasticity theory. They also examined the surface free energy effect on the nonlinear buckling and postbuckling behavior of cylindrical nanoshells under a combination of axial compressive load and hydrostatic pressure [42]. Recently, Sahmani et al. [43] anticipated the buckling and postbuckling behavior of hydrostatic pressurized cylindrical nanoshells based upon the surface elasticity theory.

In the present investigation, for the first time, the role of surface stress in the nonlinear buckling and postbuckling behaviors of cylindrical nanoshells subjected to two different radial compressions including lateral pressure and hydrostatic pressure is predicted and compared to each other. To this end, Gurtin-Murdoch elasticity theory is implemented into the classical shell theory to develop a non-classical shell model which has the capability to capture surface effects efficiently. The non-classical governing differential equations with von Karman-Donnell-type of kinematic nonlinearity are derived based on virtual work's principle. Afterwards, by using a boundary layer theory and a two-stepped singular perturbation technique, the size-dependent critical buckling load and the postbuckling equilibrium paths of perfect cylindrical nanoshells subjected to both lateral and hydrostatic pressures are obtained.

## 2. Mathematical formulations

Consider a cylindrical nanoshell of length $L$, mid-surface radius$R$, and thickness $h$ subjected to a radial compressive load. A curvilinear coordinate system $(x, y, z)$ is attached to the nanoshell as the $x$-axis is taken along the length of the shell as shown in Fig. 1.

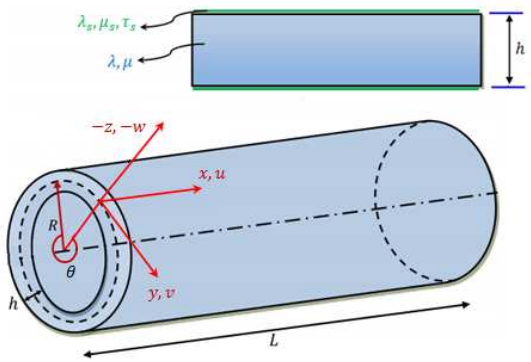


**Fig. 1.** Schematic view of a cylindrical nanoshell with surface layers

The nanoshell includes a bulk part and two additional thin surface layers (inner and outer layers).For the bulk part, the material properties are Young's modulus $E$ and Poisson's ratio $\nu$. Based on the classical shell

theory, the displacement field can be expressed as

$$u_x(x,y,z) = u(x,y) - z\frac{\partial w(x,y)}{\partial x} \quad (1a)$$

$$u_y(x,y,z) = v(x,y) - z\frac{\partial w(x,y)}{\partial y} \quad (1b)$$

$$u_z(x,y,z) = w(x,y) \quad (1c)$$

in which $u$, $v$ and $w$ represent the middle surface displacements along $x, y$ and $z$ axis, respectively.

Following the von Karman-Donnell-type kinematics of nonlinearity [44], which is on the basis of this stipulation that the thickness of the shell $h$, is remarkably small in comparison with its radius of curvature $R$, the kinematical strain-displacement relationships can be written as follow

$$\begin{Bmatrix}\varepsilon_{xx}\\ \varepsilon_{yy}\\ \gamma_{xy}\end{Bmatrix} = \begin{Bmatrix}\varepsilon^0_{xx}\\ \varepsilon^0_{yy}\\ \gamma^0_{xy}\end{Bmatrix} + z\begin{Bmatrix}\kappa_{xx}\\ \kappa_{yy}\\ \kappa_{xy}\end{Bmatrix} = \begin{Bmatrix}\frac{\partial u}{\partial x} + \frac{1}{2}\left(\frac{\partial w}{\partial x}\right)^2\\ \frac{\partial v}{\partial y} - \frac{w}{R} + \frac{1}{2}\left(\frac{\partial w}{\partial y}\right)^2\\ \frac{\partial u}{\partial y} + \frac{\partial v}{\partial x} + \frac{\partial w}{\partial x}\frac{\partial w}{\partial y}\end{Bmatrix} - z\begin{Bmatrix}\frac{\partial^2 w}{\partial x^2}\\ \frac{\partial^2 w}{\partial y^2}\\ 2\frac{\partial^2 w}{\partial x \partial y}\end{Bmatrix} \quad (2)$$

where $\varepsilon^0_{xx}, \varepsilon^0_{xx}, \gamma^0_{xy}$ stand for the strain components of the middle surface, and $\kappa_{xx}, \kappa_{yy}, \kappa_{xy}$ denote the curvature components of nanoshell.

Then, the constitutive relations can be given as

$$\begin{Bmatrix}\sigma_{xx}\\ \sigma_{yy}\\ \sigma_{xy}\end{Bmatrix} = \begin{bmatrix}\lambda+2\mu & \lambda & 0\\ \lambda & \lambda+2\mu & 0\\ 0 & 0 & \mu\end{bmatrix}\begin{Bmatrix}\varepsilon_{xx}\\ \varepsilon_{yy}\\ \gamma_{xy}\end{Bmatrix} \quad (3)$$

in which

$\lambda = E\nu/(1-\nu^2), \mu = E/\big(2(1+\nu)\big)$are Lame's constants.

Gurtin-Murdoch elasticity theory facilitates considering surface energy effects in the conventional continuum approach. In relation with the atomic features of nanostructures, there are always interactions between the elastic surface and bulk material. As a result, nanostructures mostly undergo in-plane loads in various directions. These in-plane loads on the surfaces of the bulk of nanoshell leads to surface stresses which can be obtained by using surface constitutive equations of Gurtin-Murdoch elasticity theory as follow [24,25]

$$\sigma^s_{ij} = \tau_s\delta_{ij} + (\tau_s+\lambda_s)\varepsilon_{kk}\delta_{ij} + 2(\mu_s-\tau_s)\varepsilon_{ij} + \tau_s u^s_{i,j} \quad (4)$$

$$\sigma^s_{iz} = \tau_s u^s_{z,i}$$

$$(i,j = x,y)$$

where $\lambda_s$ and $\mu_s$ represent the surface Lame's constants and $\tau_s$ is the residual surface stress under unstrained conditions. As a result, the components of surface stress can be determined with respect to the displacement components as below

$$\begin{aligned}
&\sigma^s_{xx} = (\lambda_s+2\mu_s)\varepsilon_{xx} + (\tau_s+\lambda_s)\varepsilon_{yy} + \tau_s - \frac{\tau_s}{2}\left(\frac{\partial w}{\partial x}\right)^2\\
&\sigma^s_{yy} = (\lambda_s+2\mu_s)\varepsilon_{yy} + (\tau_s+\lambda_s)\varepsilon_{xx} + \frac{\tau_s}{R}w + \tau_s - \frac{\tau_s}{2}\left(\frac{\partial w}{\partial y}\right)^2\\
&\sigma^s_{xy} = \mu_s\gamma_{xy} - \tau_s\left(\frac{\partial v}{\partial x} + \frac{\partial w}{\partial x}\frac{\partial w}{\partial y} - z\frac{\partial^2 w}{\partial x\partial y}\right)\\
&\sigma^s_{yx} = \mu_s\gamma_{xy} - \tau_s\left(\frac{\partial u}{\partial y} + \frac{\partial w}{\partial x}\frac{\partial w}{\partial y} - z\frac{\partial^2 w}{\partial x\partial y}\right)\\
&\sigma^s_{xz} = \tau_s\frac{\partial w}{\partial x} \quad , \quad \sigma^s_{yz} = \tau_s\frac{\partial w}{\partial y}
\end{aligned} \quad (5)$$

In the classical theories, as the stress component $\sigma_{zz}$ is small compared to the other normal stresses, it is assumed that $\sigma_{zz} = 0$. Nevertheless, this assumption does not satisfy the surface conditions related to the Gurtin-Murdoch model. To tackle this problem, it is supposed that the stress component $\sigma_{zz}$ varies linearly through the thickness and satisfies the balance conditions on the surfaces of nanoshell. According to this assumption, $\sigma_{zz}$ can be obtained as [45].

$$\sigma_{zz} = \frac{\left(\frac{\partial\sigma^{S+}_{xz}}{\partial x} + \frac{\partial\sigma^{S+}_{yz}}{\partial y}\right) - \left(\frac{\partial\sigma^{S-}_{xz}}{\partial x} + \frac{\partial\sigma^{S-}_{yz}}{\partial y}\right)}{2} + \frac{\left(\frac{\partial\sigma^{S+}_{xz}}{\partial x} + \frac{\partial\sigma^{S+}_{yz}}{\partial y}\right) + \left(\frac{\partial\sigma^{S-}_{xz}}{\partial x} + \frac{\partial\sigma^{S-}_{yz}}{\partial y}\right)}{h} z \quad (6)$$

in which the superscripts $S^+$ and $S^-$refer to the outer and inner surfaces of nanoshell, respectively. Through inserting equation (5) into equation (6), $\sigma_{zz}$can be achieved as follows

$$\sigma_{zz} = \frac{2\tau_s z}{h}\left(\frac{\partial^2 w}{\partial x^2} + \frac{\partial^2 w}{\partial y^2}\right) \quad (7)$$

Now, by consideration of $\sigma_{zz}$ in the constitutive equation (3), one will have

$$\sigma_{xx} = (\lambda+2\mu)\left(\varepsilon_{xx} + \frac{\nu}{E}\sigma_{zz}\right) + \lambda\left(\varepsilon_{yy} + \frac{\nu}{E}\sigma_{zz}\right) \quad (8a)$$

$$\sigma_{yy} = (\lambda+2\mu)\left(\varepsilon_{yy} + \frac{\nu}{E}\sigma_{zz}\right) + \lambda\left(\varepsilon_{xx} + \frac{\nu}{E}\sigma_{zz}\right) \quad (8b)$$

As a result, the normal stresses $(\sigma_{xx}, \sigma_{yy})$ for the bulk of the nanoshell can be expressed as [42].

$$\sigma_{xx} = (\lambda+2\mu)\varepsilon_{xx} + \lambda\varepsilon_{yy} + \frac{\nu\sigma_{zz}}{(1-\nu)} \quad (9a)$$

$$\sigma_{yy} = (\lambda+2\mu)\varepsilon_{yy} + \lambda\varepsilon_{xx} + \frac{\nu\sigma_{zz}}{(1-\nu)} \quad (9b)$$

Based on the continuum surface elasticity theory, the total strain energy of a cylindrical nanoshell incorporating the surface stress effects can be expressed as

$$\begin{aligned}&\Pi_s = \frac{1}{2}\int_S \int_{-\frac{h}{2}}^{\frac{h}{2}} \sigma_{ij}\varepsilon_{ij}dz\,dS + \\ &\frac{1}{2}\left(\int_{S^+} \sigma_{ij}^s \varepsilon_{ij} dS^+ + \int_{S^-} \sigma_{ij}^s \varepsilon_{ij} dS^-\right) \\ &= \frac{1}{2}\int_S \left\{\bar{N}_{xx}\varepsilon_{xx}^0 + \bar{N}_{yy}\varepsilon_{yy}^0 + \bar{N}_{xy}\gamma_{xy}^0 + \right. \\ &\bar{M}_{xx}\kappa_{xx} + \bar{M}_{yy}\kappa_{yy} + \bar{M}_{xy}\kappa_{xy} + \\ &\left. Q_x^s \frac{\partial w}{\partial x} + Q_y^s \frac{\partial w}{\partial y}\right\} dS\end{aligned} \tag{10}$$

where $S$ is the area occupied by the middle surface of the nanoshell. In equation (10), the in-plane forces, bending moments and shear forces are obtained as

$$\begin{aligned}&\bar{N}_{xx} = N_{xx} + \sigma_{xx}^{s+} + \sigma_{xx}^{s-} = A_{11}^*\varepsilon_{xx}^0 + \\ &A_{12}^*\varepsilon_{yy}^0 + 2\tau_s - \tau_s\left(\frac{\partial w}{\partial x}\right)^2 \\ &\bar{N}_{yy} = N_{yy} + \sigma_{yy}^{s+} + \sigma_{yy}^{s-} = A_{11}^*\varepsilon_{yy}^0 + \\ &A_{12}^*\varepsilon_{xx}^0 + \frac{2\tau_s}{R}w + 2\tau_s - \tau_s\left(\frac{\partial w}{\partial y}\right)^2 \\ &\bar{N}_{xy} = N_{xy} + \frac{1}{2}\left(\sigma_{xy}^{s+} + \sigma_{yx}^{s+} + \sigma_{xy}^{s-} + \right. \\ &\left.\sigma_{yx}^{s-}\right) = A_{55}^*\gamma_{xy}^0 - \tau^s\frac{\partial w}{\partial x}\frac{\partial w}{\partial y} \\ &\bar{M}_{xx} = M_{xx} + \frac{h}{2}(\sigma_{xx}^{s+} - \sigma_{xx}^{s-}) = \\ &D_{11}^*\kappa_{xx} + D_{12}^*\kappa_{yy} + E_{11}^*\left(\frac{\partial^2 w}{\partial x^2} + \frac{\partial^2 w}{\partial y^2}\right) \\ &\bar{M}_{yy} = M_{yy} + \frac{h}{2}\left(\sigma_{yy}^{s+} - \sigma_{yy}^{s-}\right) = \\ &D_{11}^*\kappa_{yy} + D_{12}^*\kappa_{xx} + E_{11}^*\left(\frac{\partial^2 w}{\partial x^2} + \frac{\partial^2 w}{\partial y^2}\right) \\ &\bar{M}_{xy} = M_{xy} + \frac{h}{4}\left(\sigma_{xy}^{s+} + \sigma_{yx}^{s+} - \sigma_{xy}^{s-} - \right. \\ &\left.\sigma_{yx}^{s-}\right) = D_{55}^*\kappa_{xy} \\ &Q_x^s = \sigma_{xz}^{s-} + \sigma_{xz}^{s+} = 2\tau_s\frac{\partial w}{\partial x} \\ &Q_y^s = \sigma_{yz}^{s-} + \sigma_{yz}^{s+} = 2\tau_s\frac{\partial w}{\partial y}\end{aligned} \tag{11}$$

Where

$$\begin{aligned}&\begin{Bmatrix}N_{xx}\\N_{yy}\\N_{xy}\end{Bmatrix} = \int_{-\frac{h}{2}}^{\frac{h}{2}}\begin{Bmatrix}\sigma_{xx}\\\sigma_{yy}\\\sigma_{xy}\end{Bmatrix}dz \\ &\begin{Bmatrix}M_{xx}\\M_{yy}\\M_{xy}\end{Bmatrix} = \int_{-\frac{h}{2}}^{\frac{h}{2}}\begin{Bmatrix}\sigma_{xx}\\\sigma_{yy}\\\sigma_{xy}\end{Bmatrix}zdz\end{aligned} \tag{12}$$

and

$$\begin{aligned}&A_{11}^* = (\lambda + 2\mu)h + 2(\lambda_s + 2\mu_s) \\ &A_{12}^* = \lambda h + 2\tau_s + 2\lambda_s \\ &A_{55}^* = \mu h + 2\mu_s - \tau_s \\ &D_{11}^* = \frac{(\lambda+2\mu)h^3}{12} + \frac{(\lambda_s+2\mu_s)h^2}{2} \\ &D_{12}^* = \frac{\lambda h^3}{12} + \frac{(\tau_s+\lambda_s)h^2}{2} \\ &E_{11}^* = \frac{\nu h^2\tau_s}{6(1-\nu)} \\ &D_{55}^* = \frac{\mu h^3}{12} + \frac{(2\mu_s-\tau_s)h^2}{4}\end{aligned} \tag{13}$$

Moreover, the work $\Pi_P$ done by the external radial load $q$ can be expressed in the following form

$$\Pi_P = \int_S qw dS \tag{14}$$

Now, by using the virtual work's principle as below

$$\delta\int_{t_1}^{t_2}(\Pi_s - \Pi_P)\,dt = 0 \tag{15}$$

and taking the variation of $u$, $v$, and $w$ and integrating by parts, the non-classical governing differential equations can be derived as

$$\frac{\partial \bar{N}_{xx}}{\partial x} + \frac{\partial \bar{N}_{xy}}{\partial y} = 0 \tag{16a}$$

$$\frac{\partial \bar{N}_{xy}}{\partial x} + \frac{\partial \bar{N}_{yy}}{\partial y} = 0 \tag{16b}$$

$$\begin{aligned}&\frac{\partial^2 \bar{M}_{xx}}{\partial x^2} + 2\frac{\partial^2 \bar{M}_{xy}}{\partial x\partial y} + \frac{\partial^2 \bar{M}_{yy}}{\partial y^2} + \frac{\partial Q_x^s}{\partial x} + \\ &\frac{\partial Q_y^s}{\partial y} + \frac{\bar{N}_{yy}}{R} + \bar{N}_{xx}\frac{\partial^2 w}{\partial x^2} + 2\bar{N}_{xy}\frac{\partial^2 w}{\partial x\partial y} + \\ &\bar{N}_{yy}\frac{\partial^2 w}{\partial y^2} + q = 0\end{aligned} \tag{16c}$$

The Airy stress function $f(x,y)$ can be defined as

$$\begin{aligned}&\bar{N}_{xx} = \frac{\partial^2 f}{\partial y^2} \\ &\bar{N}_{yy} = \frac{\partial^2 f}{\partial x^2} \\ &\bar{N}_{xy} = -\frac{\partial^2 f}{\partial x\partial y}\end{aligned} \tag{17}$$

As a result, the strain components can be expressed as below

$$\begin{aligned}&\varepsilon_{xx}^0 = -\varphi_2\frac{\partial^2 f}{\partial x^2} + \varphi_1\frac{\partial^2 f}{\partial y^2} + 2\tau_s\varphi_2\frac{w}{R} - \\ &\frac{2\tau_s}{A_{11}^*+A_{12}^*} + \tau_s\varphi_1\left(\frac{\partial w}{\partial x}\right)^2 - \tau_s\varphi_2\left(\frac{\partial w}{\partial y}\right)^2\end{aligned} \tag{18a}$$

$$\begin{aligned}&\varepsilon_{yy}^0 = -\varphi_2\frac{\partial^2 f}{\partial y^2} + \varphi_1\frac{\partial^2 f}{\partial x^2} - 2\tau_s\varphi_1\frac{w}{R} - \\ &\frac{2\tau_s}{A_{11}^*+A_{12}^*} + \tau_s\varphi_1\left(\frac{\partial w}{\partial y}\right)^2 - \tau_s\varphi_2\left(\frac{\partial w}{\partial x}\right)^2\end{aligned} \tag{18b}$$

$$\gamma_{xy}^0 = -\varphi_3\frac{\partial^2 f}{\partial x\partial y} + \tau_s\varphi_3\frac{\partial w}{\partial x}\frac{\partial w}{\partial y} \tag{18c}$$

in which

$$\begin{aligned}&\varphi_1 = \frac{A_{11}^*}{(A_{11}^*)^2-(A_{12}^*)^2} \\ &\varphi_2 = \frac{A_{12}^*}{(A_{11}^*)^2-(A_{12}^*)^2} \\ &\varphi_3 = \frac{1}{A_{55}^*}\end{aligned} \tag{19}$$

Also, the geometrical compatibility equation for a perfect cylindrical shell is written as

$$\frac{\partial^2 \varepsilon_{xx}^0}{\partial y^2}+\frac{\partial^2 \varepsilon_{yy}^0}{\partial x^2}-\frac{\partial^2 \gamma_{xy}^0}{\partial x \partial y}=\left(\frac{\partial^2 w}{\partial x \partial y}\right)^2-\frac{\partial^2 w}{\partial x^2}\frac{\partial^2 w}{\partial y^2}-\frac{1}{R}\frac{\partial^2 w}{\partial x^2} \quad (20)$$

From differential equations of (16c) and (20) and with the aid of equations (11) and (18), the nonlinear size-dependent governing differential equations can be derived as

$$\varphi_4\frac{\partial^4 w}{\partial x^4}+2\varphi_5\frac{\partial^4 w}{\partial x^2 \partial y^2}+\varphi_4\frac{\partial^4 w}{\partial y^4}-2\tau_s\left(\frac{\partial^2 w}{\partial x^2}+\frac{\partial^2 w}{\partial y^2}\right)-\frac{1}{R}\frac{\partial^2 f}{\partial x^2}=\frac{\partial^2 w}{\partial x^2}\frac{\partial^2 f}{\partial y^2}-2\frac{\partial^2 w}{\partial x \partial y}\frac{\partial^2 f}{\partial x \partial y}+\frac{\partial^2 w}{\partial y^2}\frac{\partial^2 f}{\partial x^2}+q \quad (21a)$$

$$\varphi_1\frac{\partial^4 f}{\partial x^4}+(\varphi_3-2\varphi_2)\frac{\partial^4 f}{\partial x^2 \partial y^2}+\varphi_1\frac{\partial^4 f}{\partial y^4}+\frac{2\tau_s}{R}\left(-\varphi_1\frac{\partial^2 w}{\partial x^2}+\varphi_2\frac{\partial^2 w}{\partial y^2}\right)+\frac{1}{R}\frac{\partial^2 w}{\partial x^2}=\left(\frac{\partial^2 w}{\partial x \partial y}\right)^2-\frac{\partial^2 w}{\partial x^2}\frac{\partial^2 w}{\partial y^2}-2\tau_s\varphi_1\left(\frac{\partial^3 w}{\partial x \partial y^2}\frac{\partial w}{\partial x}+2\left(\frac{\partial^2 w}{\partial x \partial y}\right)^2+\frac{\partial^3 w}{\partial x^2 \partial y}\frac{\partial w}{\partial y}\right)+2\tau_s\varphi_2\left(\frac{\partial^3 w}{\partial x^3}\frac{\partial w}{\partial x}+\frac{\partial^3 w}{\partial y^3}\frac{\partial w}{\partial y}+\left(\frac{\partial^2 w}{\partial x^2}\right)^2+\left(\frac{\partial^2 w}{\partial y^2}\right)^2\right)+\tau_s\varphi_3\left(\frac{\partial^3 w}{\partial x^2 \partial y}\frac{\partial w}{\partial y}+\frac{\partial^2 w}{\partial x^2}\frac{\partial^2 w}{\partial y^2}+\left(\frac{\partial^2 w}{\partial x \partial y}\right)^2+\frac{\partial w}{\partial x}\frac{\partial^3 w}{\partial x \partial y^2}\right) \quad (21b)$$

where

$$\varphi_4=D_{11}^*-E_{11}^*$$
$$\varphi_5=D_{12}^*+D_{55}^*-E_{11}^* \quad (22)$$

It is assumed that the end supports of nanoshell are simply supported or clamped. Therefore, the boundary conditions at $x=0,L$ can be expressed as

For clamped edge supports:

$$w=0,\frac{\partial w}{\partial x}=0$$

Also, it is clear that

$$\int_0^{2\pi R}\bar{N}_{xx}dy+\pi R^2 q\wp=0 \quad (23)$$

in which $\wp$ is equal to 0 and 1, respectively, for the lateral and hydrostatic pressure loads. The two loading cases are shown schematically in Fig. 2.

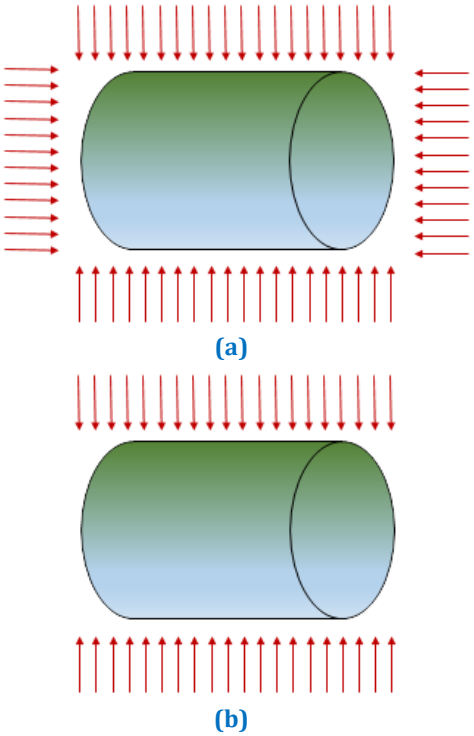


**Fig. 2.** Schematic views of loading cases: **(a)** hydrostatic pressure, **(b)** lateral pressure

Moreover, the closed condition (periodicity) can be written as

$$\int_0^{2\pi R}\frac{\partial v}{\partial y}dy=0 \quad (24a)$$

$$\int_0^{2\pi R}\left(-\varphi_2\frac{\partial^2 f}{\partial y^2}+\varphi_1\frac{\partial^2 f}{\partial x^2}-2\tau_s\varphi_1\frac{w}{R}-\frac{2\tau_s}{A_{11}^*+A_{12}^*}+\tau_s\varphi_1\left(\frac{\partial w}{\partial y}\right)^2-\tau_s\varphi_2\left(\frac{\partial w}{\partial x}\right)^2+\frac{w}{R}-\frac{1}{2}\left(\frac{\partial w}{\partial y}\right)^2\right)dy=0 \quad (24b)$$

The average end shortening of nanoshell can be introduced as

$$\frac{\Delta_x}{L}=-\frac{1}{2\pi RL}\int_0^{2\pi R}\int_0^L\frac{\partial u}{\partial x}dx\,dy=-\frac{1}{2\pi RL}\int_0^{2\pi R}\int_0^L\left(-\varphi_2\frac{\partial^2 f}{\partial x^2}+\varphi_1\frac{\partial^2 f}{\partial y^2}+2\tau_s\varphi_2\frac{w}{R}-\frac{2\tau_s}{A_{11}^*+A_{12}^*}+\tau_s\varphi_1\left(\frac{\partial w}{\partial x}\right)^2-\tau_s\varphi_2\left(\frac{\partial w}{\partial y}\right)^2-\frac{1}{2}\left(\frac{\partial w}{\partial x}\right)^2\right)dxdy \quad (25)$$

## 3. Solution procedure

### 3.1. Boundary layer-type governing equations

In order to perform the solution methodology, the following dimensionless parameters are

defined

$$X=\frac{\pi x}{L}, Y=\frac{y}{R}, \beta=\frac{L}{\pi R}, \eta=\frac{L^2}{\pi^2 h^2}, \epsilon=\frac{\pi^2 R h}{L^2}$$
$$\{a_{11}^*, a_{12}^*, a_{55}^*, d_{11}^*, d_{12}^*, d_{55}^*, e_{11}^*\}=\left\{\frac{A_{11}^*}{A_{110}}, \frac{A_{12}^*}{A_{110}}, \frac{A_{55}^*}{A_{110}}, \frac{D_{11}^*}{A_{110}h^2}, \frac{D_{12}^*}{A_{110}h^2}, \frac{D_{55}^*}{A_{110}h^2}, \frac{E_{11}^*}{A_{110}h^2}\right\} \quad (26)$$
$$W=\frac{\epsilon w}{h} \quad , \quad F=\frac{\epsilon^2 f}{A_{110}h^2} \quad , \quad \bar{\tau}=\frac{\tau_s}{A_{110}}$$
$$\mathcal{P}_q=\frac{3^{3/4}qLR^{3/2}}{4\pi A_{110}h^{3/2}} \quad , \quad \delta_q=\frac{3^{3/4}\Delta_x\sqrt{R}}{4\pi h^{3/2}}$$

in which $A_{110}=(\lambda+2\mu)h$. Now, by introducing the derivative operators as below

$$\mathcal{L}_{11}=\vartheta_4\frac{\partial^4}{\partial X^4}+2\vartheta_5\beta^2\frac{\partial^4}{\partial X^2\partial Y^2}+\vartheta_4\beta^4\frac{\partial^4}{\partial Y^4}$$
$$\mathcal{L}_{12}=-\eta\frac{\partial^2}{\partial X^2}-\eta\beta^2\frac{\partial^2}{\partial Y^2}$$
$$\mathcal{L}_{21}=\vartheta_1\frac{\partial^4}{\partial X^4}+(\vartheta_3-2\vartheta_2)\beta^2\frac{\partial^4}{\partial X^2\partial Y^2}+\vartheta_1\beta^4\frac{\partial^4}{\partial Y^4}$$
$$\mathcal{L}_{22}=-\vartheta_1\frac{\partial^2}{\partial X^2}+\vartheta_2\beta^2\frac{\partial^2}{\partial Y^2}$$
$$\tilde{\mathcal{L}}_1=\frac{\partial^2}{\partial X^2}\frac{\partial^2}{\partial Y^2}-2\frac{\partial^2}{\partial X\partial Y}\frac{\partial^2}{\partial X\partial Y}+\frac{\partial^2}{\partial Y^2}\frac{\partial^2}{\partial X^2} \quad (27)$$
$$\tilde{\mathcal{L}}_2=\frac{\partial^3}{\partial X\partial Y^2}\frac{\partial}{\partial X}+\frac{\partial}{\partial X}\frac{\partial^3}{\partial X\partial Y^2}+4\frac{\partial^2}{\partial X\partial Y}\frac{\partial^2}{\partial X\partial Y}+\frac{\partial}{\partial Y}\frac{\partial^3}{\partial X^2\partial Y}+\frac{\partial^3}{\partial X^2\partial Y}\frac{\partial}{\partial Y}$$
$$\tilde{\mathcal{L}}_3=\frac{\partial^3}{\partial X^3}\frac{\partial}{\partial X}+\frac{\partial}{\partial X}\frac{\partial^3}{\partial X^3}+\beta^4\frac{\partial^3}{\partial Y^3}\frac{\partial}{\partial Y}+\beta^4\frac{\partial}{\partial Y}\frac{\partial^3}{\partial Y^3}+2\frac{\partial^2}{\partial X^2}\frac{\partial^2}{\partial X^2}+2\beta^4\frac{\partial^2}{\partial Y^2}\frac{\partial^2}{\partial Y^2}$$
$$\tilde{\mathcal{L}}_4=\frac{\partial^2}{\partial X^2}\frac{\partial^2}{\partial Y^2}+2\frac{\partial^2}{\partial X\partial Y}\frac{\partial^2}{\partial X\partial Y}+\frac{\partial^2}{\partial Y^2}\frac{\partial^2}{\partial X^2}+\frac{\partial^3}{\partial X^2\partial Y}\frac{\partial}{\partial Y}+\frac{\partial}{\partial Y}\frac{\partial^3}{\partial X^2\partial Y}+\frac{\partial}{\partial X}\frac{\partial^3}{\partial X\partial Y^2}+\frac{\partial^3}{\partial X\partial Y^2}\frac{\partial}{\partial X}$$

The dimensionless form of the size-dependent nonlinear governing differential equations can be expressed as

$$\epsilon^2\mathcal{L}_{11}(W)+\epsilon^2 2\bar{\tau}\mathcal{L}_{12}(W)-\frac{\partial^2 F}{\partial X^2}=\beta^2\tilde{\mathcal{L}}_1(W,F)+\epsilon^{3/2}\frac{4}{3}3^{1/4}\mathcal{P}_q \quad (28a)$$

$$\mathcal{L}_{21}(F)+2\bar{\tau}\mathcal{L}_{22}(W)+\frac{\partial^2 W}{\partial X^2}=-\frac{\beta^2}{2}\tilde{\mathcal{L}}_1(W,W)-\bar{\tau}\vartheta_1\beta^2\tilde{\mathcal{L}}_2(W,W)+\bar{\tau}\vartheta_2\tilde{\mathcal{L}}_3(W,W)+\frac{\bar{\tau}\vartheta_3\beta^2}{2}\tilde{\mathcal{L}}_4(W,W) \quad (28b)$$

where

$$\vartheta_1=\frac{a_{11}^*}{(a_{11}^*)^2-(a_{12}^*)^2}$$
$$\vartheta_2=\frac{a_{12}^*}{(a_{11}^*)^2-(a_{12}^*)^2} \quad (29)$$
$$\vartheta_3=\frac{1}{a_{55}^*}$$
$$\vartheta_4=d_{11}^*-e_{11}^*$$
$$\vartheta_5=d_{12}^*+d_{55}^*-e_{11}^*$$

Furthermore, the boundary conditions in dimensionless form will be at $X=0,\pi$

For clamped edge supports: $W=0, \frac{\partial W}{\partial X}=0$

Also, one will have

$$\frac{1}{2\pi}\int_0^{2\pi}\beta^2\frac{\partial^2 F}{\partial Y^2}dY+\frac{2}{3}3^{1/4}\epsilon^{3/2}\mathcal{P}_q\mathscr{P}=0 \quad (30)$$

and the closed condition becomes

$$\int_0^{2\pi}\left(\vartheta_1\frac{\partial^2 F}{\partial X^2}-\vartheta_2\beta^2\frac{\partial^2 F}{\partial Y^2}+(1-2\bar{\tau}\vartheta_1)W-\bar{\tau}\vartheta_2\left(\frac{\partial W}{\partial X}\right)^2-\frac{\beta^2}{2}(1-2\bar{\tau}\vartheta_1)\left(\frac{\partial W}{\partial Y}\right)^2-2\bar{\tau}\vartheta_6(\vartheta_1-\vartheta_2)\epsilon\right)dY=0 \quad (31)$$

In addition, the unit end shortening of nanoshell can be expressed as

$$\delta_q = -\frac{3^{3/4}}{8\pi^2\varepsilon^{3/2}}\int_0^{2\pi}\int_0^{\pi}\Big(\vartheta_1\beta^2\frac{\partial^2 F}{\partial Y^2} - \vartheta_2\frac{\partial^2 F}{\partial X^2} + 2\bar{\tau}\vartheta_2 W - \frac{1}{2}(1 - 2\bar{\tau}\vartheta_1)\left(\frac{\partial W}{\partial X}\right)^2 - \bar{\tau}\vartheta_2\beta^2\left(\frac{\partial W}{\partial Y}\right)^2 - 2\bar{\tau}\vartheta_6(\vartheta_1 - \vartheta_2)\epsilon\Big)\,dXdY \tag{32}$$

where $\vartheta_6 = R/h$.

### 3.2. Singular perturbation technique

In the preceding subsection, the important parameter $\epsilon$ was introduced. It has been revealed that practically, for a shell-type structure, one will always have $\epsilon \ll 1$. Therefore, equations (28) represent the boundary layer type equations which consider both nonlinear prebuckling deformations and large deflections in the postbuckling domain in conjunction with the effect of surface stress. Now, by assuming $\epsilon$ as a small perturbation parameter, the singular perturbation technique can be put to use which has been successfully applied to the nonlinear analyses of cylindrical shells at macroscale [46-54]. On the basis of this technique, it is assumed that

$$W = \bar{W}(X,Y,\epsilon) + \tilde{W}(X,Y,\epsilon,\xi) + \hat{W}(X,Y,\epsilon,\varsigma) \tag{33a}$$

$$F = \bar{F}(X,Y,\epsilon) + \tilde{F}(X,Y,\epsilon,\xi) + \hat{F}(X,Y,\epsilon,\varsigma) \tag{33b}$$

where $\bar{W}(X,Y,\epsilon), \bar{F}(X,Y,\epsilon)$ denote regular solutions of the nanoshell, $\tilde{W}(X,Y,\epsilon,\xi), \tilde{F}(X,Y,\epsilon,\xi)$ and $\hat{W}(X,Y,\epsilon,\varsigma), \hat{F}(X,Y,\epsilon,\varsigma)$ are the boundary layer solutions corresponding to $X = 0$ and $X = \pi$, respectively. These solutions can be expressed in the forms of perturbation expansions as below

$$\bar{W}(X,Y,\epsilon) = \sum_{i=0}\epsilon^{i/2}\bar{W}_{i/2}(X,Y)$$

$$\bar{F}(X,Y,\epsilon) = \sum_{i=0}\epsilon^{i/2}\bar{F}_{i/2}(X,Y)$$

$$\tilde{W}(X,Y,\epsilon,\xi) = \sum_{i=0}\epsilon^{i/2+1}\tilde{W}_{i/2+1}(X,Y,\xi)$$

$$\tilde{F}(X,Y,\epsilon,\xi) = \sum_{i=0}\epsilon^{i/2+2}\tilde{F}_{i/2+2}(X,Y,\xi) \tag{34}$$

$$\hat{W}(X,Y,\epsilon,\varsigma) = \sum_{i=0}\epsilon^{i/2+1}\hat{W}_{i/2+1}(X,Y,\varsigma)$$

$$\hat{F}(X,Y,\epsilon,\varsigma) = \sum_{i=0}\epsilon^{i/2+2}\hat{F}_{i/2+2}(X,Y,\varsigma)$$

in which $\xi$ and $\varsigma$ stand for boundary layer variables which are defined as

$$\xi = \frac{X}{\sqrt{\epsilon}} \quad , \quad \varsigma = \frac{\pi - X}{\sqrt{\epsilon}} \tag{35}$$

Furthermore, it is assumed that

$$\epsilon^{3/2}\frac{4}{3}3^{1/4}q = \sum_{i=0}\epsilon^i Q_i \tag{36}$$

By inserting equations (33) and (34) in the size-dependent nonlinear governing differential equations (28) and collecting the expressions with the same order of $\epsilon$, the sets of perturbation equations will be derived relevant to both regular and boundary layer solutions which are given in Appendix A. Afterwards, it is assumed that $\bar{W}_0(X,Y) = \mathcal{A}_{00}^{(0)}$, $\bar{W}_{1/2}(X,Y) = \bar{W}_1(X,Y) = 0$ and $\bar{W}_{3/2}(X,Y) = \mathcal{A}_{00}^{(3/2)}$ in addition to $\bar{F}_0(X,Y) = -\mathcal{B}_{00}^{(0)}\left(\beta^2X^2 + \wp\frac{Y^2}{2}\right)$, $\bar{F}_{1/2}(X,Y) = \bar{F}_{3/2}(X,Y) = 0$ and $\bar{F}_1(X,Y) = -\mathcal{B}_{00}^{(1)}\left(\beta^2X^2 + \wp\frac{Y^2}{2}\right)$. Moreover, the initial buckling mode of the nanoshell is considered as follows

$$\bar{W}_2(X,Y) = \mathcal{A}_{00}^{(2)} + \mathcal{A}_{11}^{(2)}\sin(mX)\sin(nY) \tag{37}$$

Through substitution of equation (37) into the sets of perturbation equations, the coefficients of $\bar{W}_i(X,Y)$ and $\bar{F}_i(X,Y)$ can be extracted step by step, all of which are in terms of $\mathcal{A}_{11}^{(2)}$. The obtained asymptotic solutions corresponding to clamped edge supports are given in Appendix A.

Now, by using the given boundary, equation (30), closed conditions (31) and based on the unit end shortening (32), the postbuckling equilibrium paths can be derived as below

$$\mathcal{P}_q = \frac{1}{2}3^{3/4}\epsilon^{-3/2}\left\{\mathcal{P}_q^{(0)} + \mathcal{P}_q^{(2)}\left(A_{11}^{(2)}\epsilon^2\right)^2 + \cdots\right\} \tag{38}$$

and

$$\delta_q = \delta_q^{(0)} + \delta_q^{(2)}\left(A_{11}^{(2)}\epsilon^2\right)^2 + \cdots \tag{39}$$

In accordance with the maximum dimensionless deflection of the nanoshell, $\mathcal{A}_{11}^{(2)}\epsilon^2$ is considered as the second perturbation parameter which in contrast to the first small perturbation parameter $\epsilon$, it may be large. If it is assumed that the maximum deflection occurs at the dimensionless point of $(X, Y) = (\pi/2m, \pi/2n)$, one will have

$$\mathcal{A}_{11}^{(2)}\epsilon^2 = \mathcal{W}_m + \mathcal{S}_1\mathcal{W}_m^2 + \cdots \quad (40)$$

in which $\mathcal{W}_m$ denotes the maximum dimensionless deflection of the nanoshell as

$$\mathcal{W}_m = \epsilon\frac{w_m}{h} + \mathcal{S}_2 \quad (41)$$

where the symbols $\mathcal{S}_1$ and $\mathcal{S}_2$ are given in Appendix A.

In order to determine the correct values of $m$ and $n$ corresponding to the maximum deflection, the minimum value of buckling load obtained by equation (38) should be calculated by taking $W = 0$ (note that $\mathcal{W}_m \neq 0$).

## 4. Numerical results and discussion

In this section, the postbuckling equilibrium paths of cylindrical nanoshells subjected to radial compression are presented including surface stress effects and corresponding to both lateral and hydrostatic pressure loading cases. The material properties of nanoshell made of Silicon are tabulated in Table. 1.

**Table. 1.** Material properties of a cylindrical nanoshell made of Silicon [55, 56]

| | |
|---|---|
| $E(GPa)$ | 210 |
| $\nu$ | 0.24 |
| $\mu_s(N/m)$ | -2.774 |
| $\lambda_s(N/m)$ | -4.488 |
| $\tau_s(N/m)$ | 0.6048 |

Also, in all of the preceding numerical results, it is assumed that the edge supports of nanoshells are clamped and $R/h = 50$, $L^2/Rh = 200$. At first, the validity as well as the accuracy of the present solution methodology is checked. Because in accordance with authors' knowledge, there is no investigation available in published literature in which the buckling or postbuckling behavior of nanoshells is investigated in the presence of surface stress effects, by ignoring the nonlinear and surface elasticity terms, the critical buckling load of a cylindrical shell at usual scale subjected to lateral pressure is calculated based on the present solution procedure and is compared with that of Mirfakhraei and Redekop [57] using differential quadrature numerical method. In Table. 2, the critical buckling pressures of cylindrical shells with clamped edge supports obtained by the two different methods are compared corresponding to the same material and geometric properties. A very good agreement is found which confirms the validity of the current analysis. The influence of surface stress on the dimensionless postbuckling load-deflection curves of Silicon cylindrical nanoshells with various thicknesses is shown in Fig. 3 corresponding to both lateral and hydrostatic pressure loads.

**Table. 2.** Comparison of the critical buckling pressures of isotropic cylindrical shells with clamped edge supports subjected to lateral pressure ($\nu = 0.3, E = 200\ GPa$)

| $L/R$ | $R/h$ | Present work (Pa) | Ref. [57] (Pa) |
|---|---|---|---|
| 2 | 300 | 84991.09 | 85860 |
| | 3000 | 275.82 | 276.5 |
| 5 | 300 | 32897.22 | 32954 |
| | 3000 | 108.13 | 109 |

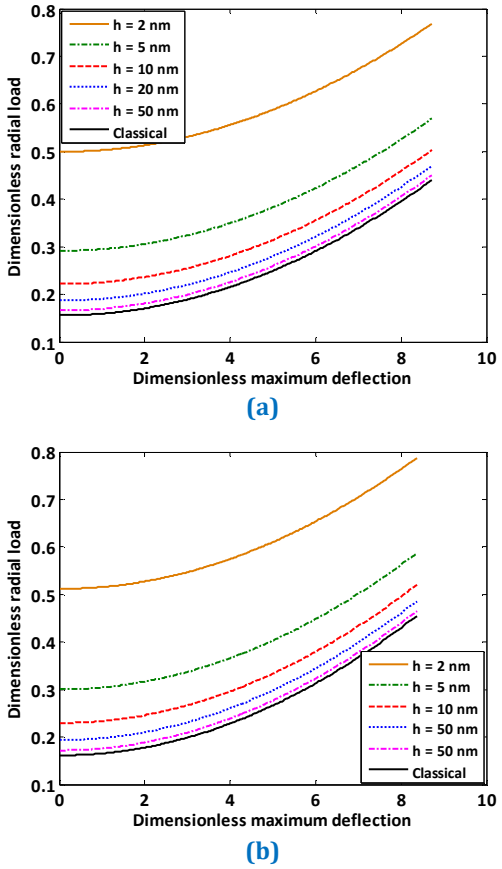


**Fig. 3.** Dimensionless postbuckling load-deflection curves of cylindrical nanoshells with different thicknesses: **(a)** hydrostatic pressure; **(b)** lateral pressure

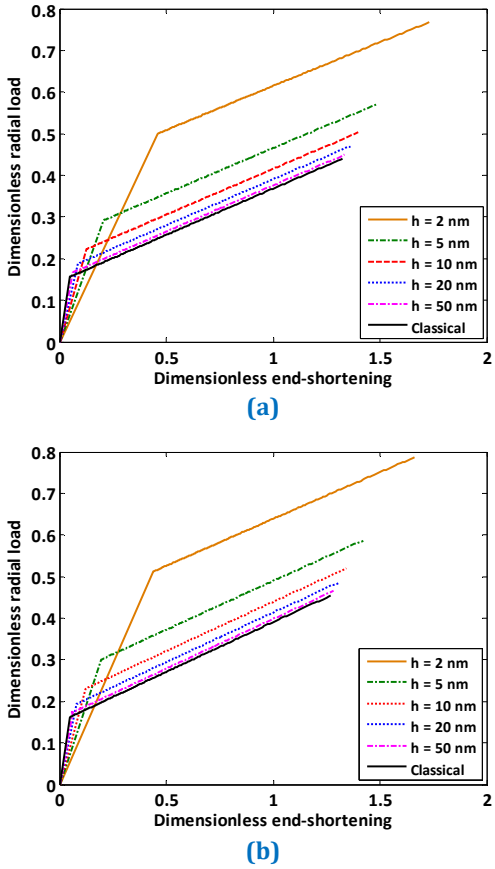


**Fig. 4.** Dimensionless postbuckling load-shortening curves of cylindrical nanoshells with different thicknesses: **(a)** hydrostatic pressure; **(b)** lateral pressure

It can be seen that the difference between predictions of the classical and non-classical shell models increases by decrease the value of shell thickness. It means that because by reduction of the shell thickness, the surface to volume ratio of nanoshell increases, surface stress effect has more significant influence on the postbuckling behavior of nanoshells with lower thickness. Also, it is found that this pattern is somedeal more considerable for the hydrostatic pressure loading case compared to the lateral pressure one. Moreover, by increasing the value of maximum deflection, the difference between postbuckling load-deflection curves corresponding to various thicknesses tends to decrease.

Fig. 4 depicts the dimensionless postbuckling load-shortening curves of cylindrical nanoshells made of Silicon obtained by the classical and non-classical shell models.

It is observed that for both lateral and hydrostatic pressure loading cases, surface stress effects cause to increase the critical buckling load and the critical end-shortening of Silicon nanoshell. In addition, the slope of the prebuckling part of the load-shortening curve decreases through considering the effects of surface stress, because the surface Lame constants related to the silicon material have a negative sign which leads to reducing the stiffness of nanoshell. Furthermore, it can be observed that in comparison to the lateral pressure, the slope of prebuckling part of the load-shortening curves is a little higher than that of the hydrostatic pressure loading.

In Fig. 5 and 6, the influence of the value of surface elastic constants on the dimensionless postbuckling load-deflection and load-shortening curves of cylindrical nanoshells is illustrated, respectively.

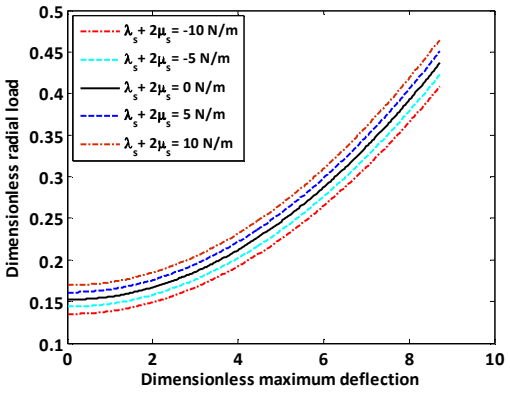


**(a)**

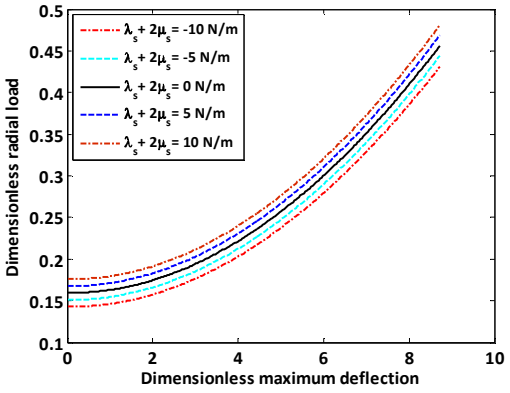


**(b)**

**Fig. 5.** Effect of surface elastic constants on the dimensionless postbuckling load-deflection curves of cylindrical nanoshells: **(a)** hydrostatic pressure; **(b)** lateral pressure ($h = 2\ nm\ , \tau_s = 0\ N/m$)

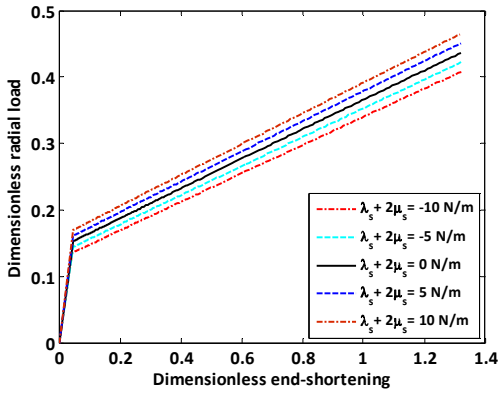


**(a)**

It is revealed that a positive value of surface elastic constants leads to increase the critical buckling load of nanoshell while a negative value causes to decrease it. In other words, surface stress effects may cause to stiffen or soften the nanoshell which depends on the sign of surface elastic constants. Additionally, in accordance with Fig. 6, it is seen that a positive value of surface elastic constants causes to increase both critical buckling load and the critical end-shortening of nanoshell which leads to higher slope for the prebuckling part of load-shortening curve.

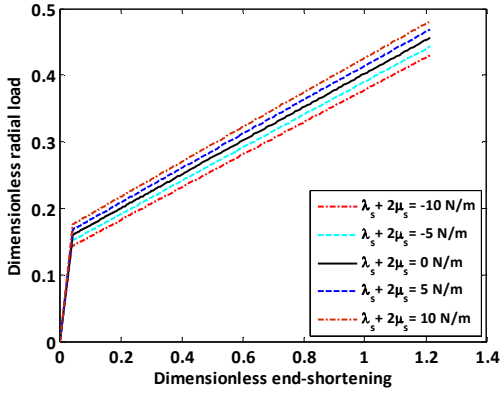


**(b)**

**Fig. 6.** Effect of surface elastic constants on the dimensionless postbuckling load-shortening curves of cylindrical nanoshells: **(a)** hydrostatic pressure; **(b)** lateral pressure ($h = 2\ nm\ , \tau_s = 0\ N/m$)

This pattern is vice versa for a negative value of surface elastic constants.

Fig. 7 and 8 demonstrate the effect of residual surface stress on the postbuckling characteristics of cylindrical nanoshells subjected to radial compressive load.

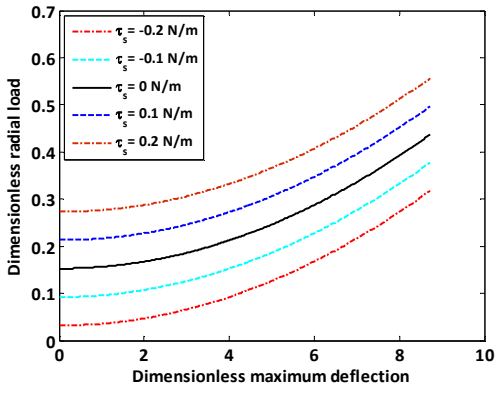


**(a)**

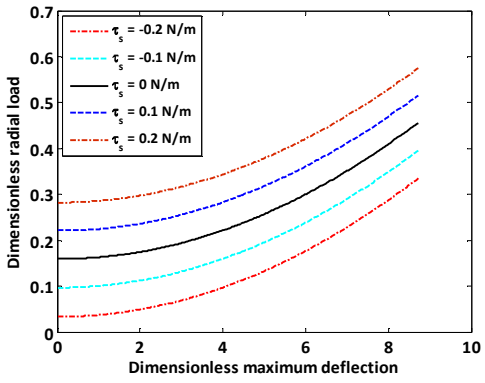


**(b)**

**Fig. 7.** Effect of residual surface stress on the dimensionless postbuckling load-deflection curves of cylindrical nanoshells: **(a)** hydrostatic pressure; **(b)** lateral pressure ($h = 2\ nm\ , \lambda_s + 2\mu_s = 0\ N/m$)

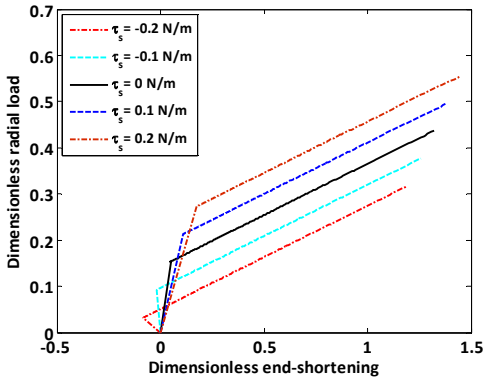


**(a)**

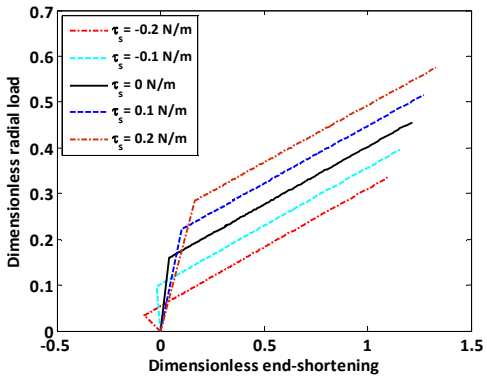


**(b)**

**Fig. 8.** Effect of residual surface stress on the dimensionless postbuckling load-shortening curves of cylindrical nanoshells: **(a)** hydrostatic pressure; **(b)** lateral pressure ($h = 2\ nm\ , \lambda_s + 2\mu_s = 0\ N/m$)

It is shown again that the residual surface stress with positive sign leads to increase both critical buckling pressure and critical end shortening of nanoshell, but a negative value has an opposite influence. Furthermore, it is revealed that due to the change in the initial positions of the atoms of structure (initial shortening), the residual surface stress has a significant influence on the slope of prebuckling part of the end-shortening curve of nanoshell subjected to radial compressive load.

## 5. Conclusion

In the present investigation, the nonlinear buckling and postbuckling behavior of cylindrical nanoshells subjected to radial compression were predicted incorporating the effects of surface stress. For this purpose, Gurtin-Murdoch elasticity theory was implemented into the classical shell theory to develop a size-dependent shell model which captures surface stress effects efficiently. On the basis of virtual work's principle and within the framework of von Karman-Donnell-type kinematics nonlinearity, the non-classical governing differential equations were derived. A boundary layer theory in conjunction with a two-stepped singular perturbation methodology was employed to solve the problem.

It was indicated that surface stress effect has more significant influence on the postbuckling behavior of Silicon nanoshells with lower thicknesses. By increase the value of deflection, the difference between postbuckling load-deflection curves corresponding to various thicknesses tends to decrease. Furthermore, it was found that for both lateral and hydrostatic pressure loading cases, the slope of the prebuckling part of the load-shortening curve decreases through considering the effects of surface stress. Also, it was revealed that surface stress effects may cause to stiffen or soften the nanoshell which depends on the sign of surface elastic constants. It was observed that a positive value of surface elastic constants causes to increase the both critical buckling load and the critical end-shortening of nanoshell which leads to higher slope for the prebuckling part of load-shortening curve. This pattern is vice versa for a negative value of surface elastic constants. Additionally, it was demonstrated that due to the change in the initial positions of the atoms of structure (initial shortening), the residual surface stress has a significant influence on the slope of prebuckling part of the end-shortening curve of nanoshell subjected to radial compressive load.

## References

[1] S. Kitipornchai, X.Q. He, K.M. Liew, 2005, Continuum model for the vibration of multilayered graphene sheets, Physical Review B 72, pp. 075443.

[2] K.M. Liew, X.Q. He, S. Kitipornchai, 2006, Predicting nanovibration of multi-layered graphene sheets embedded in an elastic matrix, Acta Material 54, pp. 4229-4236.

[3] G. Cao, X. Chen, J.W. Kysar, 2006, Thermal vibration and apparent thermal contraction of single-walled carbon nanotubes, Journal of Mechanics and Physics of Solids 54, pp. 1206-1236.

[4] C. Sansour, S. Skatulla, 2009, A strain gradient generalized continuum approach for modelling elastic scale effects, Computer Methods in Applied Mechanics and Engineering 198, pp. 1401-1412.

[5] I. Elishakoff, D. Pentaras, 2009, Fundamental natural frequencies of double-walled carbon nanotubes, Journal of Sound and Vibration 322, pp. 652-664.

[6] Y.G. Hu, K.M. Liew, Q. Wang, X.Q. He, B.I. Yakobson, 2008, Nonlocal shell model for elastic wave propagation in single- and double-walled carbon nanotubes, Journal of the Mechanics and Physics of Solids 56, pp. 3475-3485.

[7] H.-S. Shen, C.L. Zhang, 2010, Torsional buckling and postbuckling of double-walled carbon nanotubes by nonlocal shear deformable shell model, Composite Structures 92, pp. 1073-1084.

[8] B. Wang, J. Zhao, Sh. Zhou, 2010, A micro scale Timoshenko beam model based on strain gradient elasticity theory, European Journal of Mechanics – A/Solids 29, pp. 591-599.

[9] R. Ansari, S. Sahmani, B. Arash, 2010, Nonlocal plate model for free vibrations of single-layered graphene sheets, Physics Letters A 375, pp. 53-62.

[10] R. Ansari, S. Sahmani, 2012, Small scale effect on vibrational response of single-walled carbon nanotubes with different boundary conditions based on nonlocal beam models, Communications in Nonlinear Science and Numerical Simulation 17, pp. 1965-1979.

[11] E. Ghavanloo, S. Ahmad Fazelzadeh, 2013, Nonlocal elasticity theory for radial vibration of nanoscale spherical shells, European Journal of Mechanics – A/Solids 41, pp. 37-42.

[12] S. Sahmani, R. Ansari, 2013, Size-dependent buckling analysis of functionally graded third-order shear deformable microbeams including thermal environment effect, Applied Mathematical Modelling 37, pp. 9499-9515.

[13] S. Sahmani, R. Ansari, 2013, On the free vibration response of functionally graded higher-order shear deformable microplates based on the strain gradient elasticity theory, Composite Structures 95, pp. 430-442.

[14] H.-S. Shen, 2013, Nonlocal shear deformable shell model for torsional buckling and postbuckling of microtubules in thermal environment, Mechanics Research Communications 54, pp. 83-95.

[15] H. Zeighampour, Y. Yadi Beni, 2014, Cylindrical thin-shell model based on modified strain gradient theory, International Journal of Engineering Science 78, pp. 27-47.

[16] S. Sahmani, M. Bahrami, R. Ansari, 2014, Nonlinear free vibration analysis of functionally graded third-order shear deformable microbeams based on the modified strain gradient elasticity theory, Composite Structures 110, pp. 219-230.

[17] K. Mercan, O. Civalek, 2017, Buckling analysis of Silicon carbide nanotubes (SiCNTs) with surface effect and nonlocal elasticity using the method of HDQ, Composites Part B: Engineering 114, pp. 34-45.

[18] S. Sahmani, M.M. Aghdam, 2017, Size dependency in axial postbuckling behavior of hybrid FGM exponential shear deformable nanoshells based on the nonlocal elasticity theory, Composite Structures 166, pp. 104-113.

[19] S. Sahmani, M.M. Aghdam, 2017, Nonlinear instability of hydrostatic pressurized hybrid FGM exponential shear deformable nanoshells based on nonlocal continuum elasticity, Composites Part B: Engineering 114, pp. 404-417.

[20] S. Sahmani, M.M. Aghdam, 2017, Temperature-dependent nonlocal instability of hybrid FGM exponential shear deformable nanoshells including imperfection sensitivity, International Journal of Mechanical Sciences 122, pp. 129-142.

[21] F.H. Streitz, R.C. Cammarata, K. Sieradzki, 1994, Surface stress effects on elastic properties, I. Thin metal films, Physical Review B 49, pp. 10699-10706.

[22] R. Dingreville, J. Qu, M. Cherkaoui, 2005, Surface free energy and its effects on the elastic behavior of nano-sized particles, wires and films, Journal of Mechanics and Physics of Solids 53, pp. 1827-1954.

[23] F.D. Fischer, T. Waitz, D. Vollath, N.K. Simha, 2008, On the role of surface energy and surface stress in phase-transforming nanoparticles, Progress in Material Science 53, pp. 481-527.

[24] M.E. Gurtin, A.I. Murdoch, 1975, A continuum theory of elastic material surface, Archive for Rational Mechanics and Analysis 57, pp. 291-323.

[25] M.E. Gurtin, A.I. Murdoch, 1978, Surface stress in solids, International Journal of Solids and Structures 14, pp. 431-440.

[26] G.-F. Wang, X.-Q. Feng, 2007, Effects of surface elasticity and residual surface tension on the natural frequency of microbeams, Applied Physics Letters 90, pp. 231904-231903.

[27] S. Abbasion, A. Rafsanjani, R. Avazmohammadi, A. Farshidianfar, 2009, Free vibration of microscaled Timoshenko beams, Applied

Physics Letters 95, pp. 143122-143123.

[28] L. Tian, R.K.N.D. Rajapakse, 2007, Elastic field of an isotropic matrix with a nanoscale elliptical inhomogeneity, International Journal of Solids and Structures 44, pp. 7988-8005.

[29] C.F. Lü, W.Q. Chen, C.W. Lim,2009, Elastic mechanical behavior of nano-scaled FGM films incorporating surface energies, Composite Science and Technology 69, pp. 1124–1130.

[30] X.J. Zhao, R.K.N.D. Rajapakse, 2009, Analytical solutions for a surface loaded isotropic elastic layer with surface energy effects, International Journal of Engineering Science 47, pp. 1433-1444.

[31] Y. Fu, J. Zhang, Y. Jiang, 2010, Influences of surface energies on the nonlinear static and dynamic behaviors of nanobeams, Physica E 42, pp. 2268-2273.

[32] R. Ansari, S. Sahmani, 2011, Bending behavior and buckling of nanobeams including surface stress effects corresponding to different beam theories, International Journal of Engineering Science, 49, pp. 1244-1255.

[33] R. Ansari, S. Sahmani, 2011, Surface stress effects on the free vibration behavior of nanoplates, International Journal of Engineering Science 49, pp. 1204-1215.

[34] R. Ansari, V. Mohammadi, M. Faghih Shojaei, R. Gholami, S. Sahmani, 2013,Postbuckling characteristics of nanobeams based on the surface elasticity theory, Composites Part B: Engineering 55, pp. 240-246.

[35] R. Ansari, V. Mohammadi, M. Faghih Shojaei, R. Gholami, S. Sahmani, 2014, Postbuckling analysis of Timoshenko nanobeams including surface stress effect, International Journal of Engineering Science 75, pp. 1-10.

[36] R. Ansari, R. Gholami,M. Faghih Shojaei,V. Mohammadi, S. Sahmani, 2014, Surface stress effect on the pull-in instability of circular nanoplates, Acta Astronautica 102, pp. 140-150.

[37] S. Sahmani, M. Bahrami, R. Ansari, 2014, Surface energy effects on the free vibration characteristics of postbuckled third-order shear deformable nanobeams, Composite Structures 116, pp. 552-561.

[38] S. Sahmani, M. Bahrami, M.M. Aghdam, R. Ansari, 2014, Surface effects on the nonlinear forced vibration response of third-order shear deformable nanobeams, Composite Structures 118, pp. 149-158.

[39] S. Sahmani, M. Bahrami, R. Ansari, 2014, Surface effects on the free vibration behavior of postbuckled circular higher-order shear deformable nanoplates including geometrical nonlinearity, Acta Astronautica 105, pp. 417-427.

[40] C.-H. Cheng, T. Chen, 2015, Size-dependent resonance and buckling behavior of nanoplates with high-order surface stress effects, Physica E 67, pp. 12-17.

[41] S. Sahmani, M.M. Aghdam, M. Bahrami, 2015, On the free vibration characteristics of postbuckled third-order shear deformable FGM nanobeams including surface effects, Composite Structures 121, pp. 377-385.

[42] S. Sahmani, M.M. Aghdam, M. Bahrami, 2015, Nonlinear buckling and postbuckling behavior of cylindrical nanoshells subjected to combined axial and radial compressions incorporating surface stress effects, Composites Part B: Engineering 79, pp. 676-691.

[43] S. Sahmani, M.M. Aghdam, M. Bahrami, 2017, Nonlinear buckling and postbuckling behavior of cylindrical shear deformable nanoshells subjected to radial compression including surface free energy effects, Acta Mechanica Solida Sinica, Article In Press.

[44] L.H. Donnell, 1976, Beam, plates and shells, McGraw-Hill, New York, USA, pp. 377-445.

[45] P. Lu, L.H. He, H.P. Lee, C. Lu, 2006, Thin plate theory including surface effects, International Journal of Solids and Structures 43, pp. 4631-4647.

[46] H.-S. Shen, T.-Y. Chen, 1988, A boundary layer theory for the buckling of thin cylindrical shells under external pressure, Applied Mathematics and Mechanics 9, pp. 557-571.

[47] H.-S. Shen, T.-Y. Chen, 1991, Buckling and postbuckling of cylindrical shells under combined external pressure and axial compression, Thin-Walled Structures 12, pp. 321-334.

[48] H.-S. Shen, 2008, Boundary layer theory for the buckling and postbuckling of an anisotropic laminated cylindrical shell. Part II: Prediction under external pressure, Composite Structures 82, pp. 362-370.

[49] H.-S. Shen, Y. Xiang, 2013, Postbuckling of nanotube-reinforced composite cylindrical shells under combined axial and radial mechanical loads in thermal environment, Composites Part B: Engineering 52, pp. 311-322.

[50] S. Sahmani, M.M. Aghdam, 2017, Imperfection sensitivity of the size-dependent postbuckling response of pressurized FGM nanoshells in thermal environments, Archives of Civil and Mechanical Engineering 17, pp. 623-638.

[51] S. Sahmani, A.M. Fattahi, 2018, Small scale effects on buckling and postbuckling behaviors

of axially loaded FGM nanoshells based on nonlocal strain gradient elasticity theory, Applied Mathematics and Mechanics 39, pp. 561-580.

[52] S. Sahmani, M.M. Aghdam, 2018, Thermo-electro-radial coupling nonlinear instability of piezoelectric shear deformable nanoshells via nonlocal elasticity theory, Microsystem Technologies 24, pp. 1333-1346.

[53] S. Sahmani, A.M. Fattahi, 2018, Development of efficient size-dependent plate models for axial buckling of single-layered graphene nanosheets using molecular dynamics simulation, Microsystem Technologies 24, pp. 1265-1277.

[54] S. Sahmani, M.M. Aghdam, 2018, Nonlinear instability of hydrostatic pressurized microtubules surrounded by cytoplasm of a living cell including nonlocality and strain gradient microsize dependency, Acta Mechanica 229, pp. 403-420.

[55] R.E. Miller, V.B. Shenoy, 2000, Size-dependent elastic properties of nanosized structural elements, Nanotechnology 11, pp. 139-147.

[56] R. Zhu, E. Pan, P.W. Chung, X. Cai, K.M. Liew, A. Buldum, 2006, Atomistic calculation of elastic moduli in strained silicon, Semiconductor Science and Technology 21, 906-911.

[57] P. Mirfakhraei, D. Redekop, 1998, Buckling of circular cylindrical shells by the differential quadrature method, International Journal of Pressure Vessels and Piping 75, pp. 347-353.

## Appendix A

The sets of perturbation equations for the regular solution are:

$$O(\epsilon^0):\begin{cases}-\dfrac{\partial^2\bar{F}_0}{\partial X^2}=\beta^2\tilde{\mathcal{L}}_1(\bar{W}_0,\bar{F}_0)+\mathcal{Q}_0\\ \mathcal{L}_{21}(\bar{F}_0)+2\bar{\tau}\mathcal{L}_{22}(\bar{W}_0)+\dfrac{\partial^2\bar{W}_0}{\partial X^2}=-\dfrac{\beta^2}{2}\tilde{\mathcal{L}}_1(\bar{W}_0,\bar{W}_0)-\bar{\tau}\vartheta_1\beta^2\tilde{\mathcal{L}}_2(\bar{W}_0,\bar{W}_0)+\bar{\tau}\vartheta_2\tilde{\mathcal{L}}_3(\bar{W}_0,\bar{W}_0)\\ \qquad\qquad+\dfrac{\bar{\tau}\vartheta_3\beta^2}{2}\tilde{\mathcal{L}}_4(\bar{W}_0,\bar{W}_0)\end{cases}$$

$$O(\epsilon^{1/2}):\begin{cases}-\dfrac{\partial^2\bar{F}_{1/2}}{\partial X^2}=\beta^2\tilde{\mathcal{L}}_1(\bar{W}_{1/2},\bar{F}_0)+\beta^2\tilde{\mathcal{L}}_1(\bar{W}_0,\bar{F}_{1/2})\\ \mathcal{L}_{21}(\bar{F}_{1/2})+2\bar{\tau}\mathcal{L}_{22}(\bar{W}_{1/2})+\dfrac{\partial^2\bar{W}_{1/2}}{\partial X^2}=-\dfrac{\beta^2}{2}\tilde{\mathcal{L}}_1(\bar{W}_0,\bar{W}_{1/2})-\bar{\tau}\vartheta_1\beta^2\tilde{\mathcal{L}}_2(\bar{W}_0,\bar{W}_{1/2})\\ \qquad\qquad+\bar{\tau}\vartheta_2\tilde{\mathcal{L}}_3(\bar{W}_0,\bar{W}_{1/2})+\dfrac{\bar{\tau}\vartheta_3\beta^2}{2}\tilde{\mathcal{L}}_4(\bar{W}_0,\bar{W}_{1/2})\end{cases}$$

$$O(\epsilon^1):\begin{cases}-\dfrac{\partial^2\bar{F}_1}{\partial X^2}=\beta^2\tilde{\mathcal{L}}_1(\bar{W}_{1/2},\bar{F}_{1/2})+\beta^2\tilde{\mathcal{L}}_1(\bar{W}_1,\bar{F}_0)+\beta^2\tilde{\mathcal{L}}_1(\bar{W}_0,\bar{F}_1)+\mathcal{Q}_1\\ \mathcal{L}_{21}(\bar{F}_1)+2\bar{\tau}\mathcal{L}_{22}(\bar{W}_1)+\dfrac{\partial^2\bar{W}_1}{\partial X^2}=-\dfrac{\beta^2}{2}\tilde{\mathcal{L}}_1(\bar{W}_0,\bar{W}_1)-\dfrac{\beta^2}{2}\tilde{\mathcal{L}}_1(\bar{W}_{1/2},\bar{W}_{1/2})-\bar{\tau}\vartheta_1\beta^2\tilde{\mathcal{L}}_2(\bar{W}_0,\bar{W}_1)\\ \qquad\qquad-\bar{\tau}\vartheta_1\beta^2\tilde{\mathcal{L}}_2(\bar{W}_{1/2},\bar{W}_{1/2})+\bar{\tau}\vartheta_2\tilde{\mathcal{L}}_3(\bar{W}_0,\bar{W}_1)+\bar{\tau}\vartheta_2\tilde{\mathcal{L}}_3(\bar{W}_{1/2},\bar{W}_{1/2})+\dfrac{\bar{\tau}\vartheta_3\beta^2}{2}\tilde{\mathcal{L}}_4(\bar{W}_0,\bar{W}_1)\\ \qquad\qquad+\dfrac{\bar{\tau}\vartheta_3\beta^2}{2}\tilde{\mathcal{L}}_4(\bar{W}_{1/2},\bar{W}_{1/2})\end{cases}$$

$$O(\epsilon^{3/2}):\begin{cases}-\dfrac{\partial^2\bar{F}_{3/2}}{\partial X^2}=\beta^2\tilde{\mathcal{L}}_1(\bar{W}_0,\bar{F}_{3/2})+\beta^2\tilde{\mathcal{L}}_1(\bar{W}_{1/2},\bar{F}_1)+\beta^2\tilde{\mathcal{L}}_1(\bar{W}_1,\bar{F}_{1/2})+\beta^2\tilde{\mathcal{L}}_1(\bar{W}_{3/2},\bar{F}_0)\\ \mathcal{L}_{21}(\bar{F}_{3/2})+2\bar{\tau}\mathcal{L}_{22}(\bar{W}_{3/2})+\dfrac{\partial^2\bar{W}_{3/2}}{\partial X^2}=-\dfrac{\beta^2}{2}\tilde{\mathcal{L}}_1(\bar{W}_0,\bar{W}_{3/2})-\dfrac{\beta^2}{2}\tilde{\mathcal{L}}_1(\bar{W}_{1/2},\bar{W}_1)\\ \qquad\qquad-\bar{\tau}\vartheta_1\beta^2\tilde{\mathcal{L}}_2(\bar{W}_0,\bar{W}_{3/2})-\bar{\tau}\vartheta_1\beta^2\tilde{\mathcal{L}}_2(\bar{W}_{1/2},\bar{W}_1)+\bar{\tau}\vartheta_2\tilde{\mathcal{L}}_3(\bar{W}_0,\bar{W}_{3/2})+\bar{\tau}\vartheta_2\tilde{\mathcal{L}}_3(\bar{W}_{1/2},\bar{W}_1)\\ \qquad\qquad+\dfrac{\bar{\tau}\vartheta_3\beta^2}{2}\tilde{\mathcal{L}}_4(\bar{W}_0,\bar{W}_{3/2})+\dfrac{\bar{\tau}\vartheta_3\beta^2}{2}\tilde{\mathcal{L}}_4(\bar{W}_{1/2},\bar{W}_1)\end{cases}$$

$$O(\epsilon^2):\begin{cases}\mathcal{L}_{11}(\bar{W}_0)+2\bar{\tau}\mathcal{L}_{12}(\bar{W}_0)-\dfrac{\partial^2\bar{F}_2}{\partial X^2}=\beta^2\tilde{\mathcal{L}}_1(\bar{W}_0,\bar{F}_2)+\beta^2\tilde{\mathcal{L}}_1\left(\bar{W}_{1/2},\bar{F}_{3/2}\right)+\beta^2\tilde{\mathcal{L}}_1(\bar{W}_1,\bar{F}_1)\\ \quad+\beta^2\tilde{\mathcal{L}}_1\left(\bar{W}_{3/2},\bar{F}_{1/2}\right)+\beta^2\tilde{\mathcal{L}}_1(\bar{W}_2,\bar{F}_0)+Q_2\\ \mathcal{L}_{21}(\bar{F}_2)+2\bar{\tau}\mathcal{L}_{22}(\bar{W}_2)+\dfrac{\partial^2\bar{W}_2}{\partial X^2}=-\dfrac{\beta^2}{2}\tilde{\mathcal{L}}_1(\bar{W}_0,\bar{W}_2)-\dfrac{\beta^2}{2}\tilde{\mathcal{L}}_1\left(\bar{W}_{1/2},\bar{W}_{3/2}\right)-\dfrac{\beta^2}{2}\tilde{\mathcal{L}}_1(\bar{W}_1,\bar{W}_1)\\ \quad-\bar{\tau}\vartheta_1\beta^2\tilde{\mathcal{L}}_2(\bar{W}_0,\bar{W}_2)-\bar{\tau}\vartheta_1\beta^2\tilde{\mathcal{L}}_2\left(\bar{W}_{1/2},\bar{W}_{3/2}\right)-\bar{\tau}\vartheta_1\beta^2\tilde{\mathcal{L}}_2(\bar{W}_1,\bar{W}_1)+\bar{\tau}\vartheta_2\tilde{\mathcal{L}}_3(\bar{W}_0,\bar{W}_2)\\ \quad+\bar{\tau}\vartheta_2\tilde{\mathcal{L}}_3(\bar{W}_{1/2},\bar{W}_{3/2})+\bar{\tau}\vartheta_2\tilde{\mathcal{L}}_3(\bar{W}_1,\bar{W}_1)+\dfrac{\bar{\tau}\vartheta_3\beta^2}{2}\tilde{\mathcal{L}}_4(\bar{W}_0,\bar{W}_2)+\dfrac{\bar{\tau}\vartheta_3\beta^2}{2}\tilde{\mathcal{L}}_4\left(\bar{W}_{1/2},\bar{W}_{3/2}\right)\\ \quad+\dfrac{\bar{\tau}\vartheta_3\beta^2}{2}\tilde{\mathcal{L}}_4(\bar{W}_1,\bar{W}_1)\end{cases}$$

$$O\left(\epsilon^{5/2}\right):\begin{cases}\mathcal{L}_{11}\left(\bar{W}_{1/2}\right)+2\bar{\tau}\mathcal{L}_{12}\left(\bar{W}_{1/2}\right)-\dfrac{\partial^2\bar{F}_{5/2}}{\partial X^2}=\beta^2\tilde{\mathcal{L}}_1\left(\bar{W}_0,\bar{F}_{5/2}\right)+\beta^2\tilde{\mathcal{L}}_1\left(\bar{W}_{1/2},\bar{F}_2\right)+\beta^2\tilde{\mathcal{L}}_1\left(\bar{W}_1,\bar{F}_{3/2}\right)\\ \quad+\beta^2\tilde{\mathcal{L}}_1\left(\bar{W}_{3/2},\bar{F}_1\right)+\beta^2\tilde{\mathcal{L}}_1\left(\bar{W}_2,\bar{F}_{1/2}\right)+\beta^2\tilde{\mathcal{L}}_1\left(\bar{W}_{5/2},\bar{F}_0\right)\\ \mathcal{L}_{21}\left(\bar{F}_{5/2}\right)+2\bar{\tau}\mathcal{L}_{22}\left(\bar{W}_{5/2}\right)+\dfrac{\partial^2\bar{W}_{5/2}}{\partial X^2}=-\dfrac{\beta^2}{2}\tilde{\mathcal{L}}_1\left(\bar{W}_0,\bar{W}_{5/2}\right)-\dfrac{\beta^2}{2}\tilde{\mathcal{L}}_1\left(\bar{W}_{1/2},\bar{W}_2\right)\\ \quad-\dfrac{\beta^2}{2}\tilde{\mathcal{L}}_1\left(\bar{W}_1,\bar{W}_{3/2}\right)-\bar{\tau}\vartheta_1\beta^2\tilde{\mathcal{L}}_2\left(\bar{W}_0,\bar{W}_{5/2}\right)-\bar{\tau}\vartheta_1\beta^2\tilde{\mathcal{L}}_2\left(\bar{W}_{1/2},\bar{W}_2\right)-\bar{\tau}\vartheta_1\beta^2\tilde{\mathcal{L}}_2\left(\bar{W}_1,\bar{W}_{3/2}\right)\\ \quad+\bar{\tau}\vartheta_2\tilde{\mathcal{L}}_3(\bar{W}_0,\bar{W}_{5/2})+\bar{\tau}\vartheta_2\tilde{\mathcal{L}}_3(\bar{W}_{1/2},\bar{W}_2)+\bar{\tau}\vartheta_2\tilde{\mathcal{L}}_3(\bar{W}_1,\bar{W}_{3/2})+\dfrac{\bar{\tau}\vartheta_3\beta^2}{2}\tilde{\mathcal{L}}_4\left(\bar{W}_0,\bar{W}_{5/2}\right)\\ \quad+\dfrac{\bar{\tau}\vartheta_3\beta^2}{2}\tilde{\mathcal{L}}_4\left(\bar{W}_{1/2},\bar{W}_2\right)+\dfrac{\bar{\tau}\vartheta_3\beta^2}{2}\tilde{\mathcal{L}}_4\left(\bar{W}_1,\bar{W}_{3/2}\right)\end{cases}$$

$$O(\epsilon^3):\begin{cases}\mathcal{L}_{11}(\bar{W}_1)+2\bar{\tau}\mathcal{L}_{12}(\bar{W}_1)-\dfrac{\partial^2\bar{F}_3}{\partial X^2}=\beta^2\tilde{\mathcal{L}}_1(\bar{W}_0,\bar{F}_3)+\beta^2\tilde{\mathcal{L}}_1\left(\bar{W}_{1/2},\bar{F}_{5/2}\right)+\beta^2\tilde{\mathcal{L}}_1(\bar{W}_1,\bar{F}_2)\\ \quad+\beta^2\tilde{\mathcal{L}}_1\left(\bar{W}_{3/2},\bar{F}_{3/2}\right)+\beta^2\tilde{\mathcal{L}}_1(\bar{W}_2,\bar{F}_1)+\beta^2\tilde{\mathcal{L}}_1\left(\bar{W}_{5/2},\bar{F}_{1/2}\right)+\beta^2\tilde{\mathcal{L}}_1(\bar{W}_3,\bar{F}_0)+Q_3\\ \mathcal{L}_{21}(\bar{F}_3)+2\bar{\tau}\mathcal{L}_{22}(\bar{W}_3)+\dfrac{\partial^2\bar{W}_3}{\partial X^2}=-\dfrac{\beta^2}{2}\tilde{\mathcal{L}}_1(\bar{W}_0,\bar{W}_3)-\dfrac{\beta^2}{2}\tilde{\mathcal{L}}_1\left(\bar{W}_{1/2},\bar{W}_{5/2}\right)-\dfrac{\beta^2}{2}\tilde{\mathcal{L}}_1(\bar{W}_1,\bar{W}_2)\\ \quad-\dfrac{\beta^2}{2}\tilde{\mathcal{L}}_1\left(\bar{W}_{3/2},\bar{W}_{3/2}\right)-\bar{\tau}\vartheta_1\beta^2\tilde{\mathcal{L}}_2(\bar{W}_0,\bar{W}_3)-\bar{\tau}\vartheta_1\beta^2\tilde{\mathcal{L}}_2\left(\bar{W}_{1/2},\bar{W}_{5/2}\right)-\bar{\tau}\vartheta_1\beta^2\tilde{\mathcal{L}}_2(\bar{W}_1,\bar{W}_2)\\ \quad-\bar{\tau}\vartheta_1\beta^2\tilde{\mathcal{L}}_2\left(\bar{W}_{3/2},\bar{W}_{3/2}\right)+\bar{\tau}\vartheta_2\tilde{\mathcal{L}}_3(\bar{W}_0,\bar{W}_3)+\bar{\tau}\vartheta_2\tilde{\mathcal{L}}_3(\bar{W}_{1/2},\bar{W}_{5/2})+\bar{\tau}\vartheta_2\tilde{\mathcal{L}}_3(\bar{W}_1,\bar{W}_2)\\ \quad+\bar{\tau}\vartheta_2\tilde{\mathcal{L}}_3(\bar{W}_{3/2},\bar{W}_{3/2})+\dfrac{\bar{\tau}\vartheta_3\beta^2}{2}\tilde{\mathcal{L}}_4(\bar{W}_0,\bar{W}_3)+\dfrac{\bar{\tau}\vartheta_3\beta^2}{2}\tilde{\mathcal{L}}_4\left(\bar{W}_{1/2},\bar{W}_{5/2}\right)+\dfrac{\bar{\tau}\vartheta_3\beta^2}{2}\tilde{\mathcal{L}}_4(\bar{W}_1,\bar{W}_2)\\ \quad+\dfrac{\bar{\tau}\vartheta_3\beta^2}{2}\tilde{\mathcal{L}}_4\left(\bar{W}_{3/2},\bar{W}_{3/2}\right)\end{cases}$$

$$O\left(\epsilon^{7/2}\right):\begin{cases}\mathcal{L}_{11}\left(\bar{W}_{3/2}\right)+2\bar{\tau}\mathcal{L}_{12}\left(\bar{W}_{3/2}\right)-\dfrac{\partial^2\bar{F}_{7/2}}{\partial X^2}=\beta^2\tilde{\mathcal{L}}_1\left(\bar{W}_0,\bar{F}_{7/2}\right)+\beta^2\tilde{\mathcal{L}}_1\left(\bar{W}_{1/2},\bar{F}_3\right)+\beta^2\tilde{\mathcal{L}}_1\left(\bar{W}_1,\bar{F}_{5/2}\right)\\ \quad+\beta^2\tilde{\mathcal{L}}_1\left(\bar{W}_{3/2},\bar{F}_2\right)+\beta^2\tilde{\mathcal{L}}_1\left(\bar{W}_2,\bar{F}_{3/2}\right)+\beta^2\tilde{\mathcal{L}}_1\left(\bar{W}_{5/2},\bar{F}_1\right)+\beta^2\tilde{\mathcal{L}}_1\left(\bar{W}_3,\bar{F}_{1/2}\right)\\ \quad+\beta^2\tilde{\mathcal{L}}_1\left(\bar{W}_{7/2},\bar{F}_0\right)\\ \mathcal{L}_{21}\left(\bar{F}_{7/2}\right)+2\bar{\tau}\mathcal{L}_{22}\left(\bar{W}_{7/2}\right)+\dfrac{\partial^2\bar{W}_{7/2}}{\partial X^2}=-\dfrac{\beta^2}{2}\tilde{\mathcal{L}}_1\left(\bar{W}_0,\bar{W}_{7/2}\right)-\dfrac{\beta^2}{2}\tilde{\mathcal{L}}_1\left(\bar{W}_{1/2},\bar{W}_3\right)-\dfrac{\beta^2}{2}\tilde{\mathcal{L}}_1\left(\bar{W}_1,\bar{W}_{5/2}\right)\\ \quad-\dfrac{\beta^2}{2}\tilde{\mathcal{L}}_1\left(\bar{W}_{3/2},\bar{W}_2\right)-\bar{\tau}\vartheta_1\beta^2\tilde{\mathcal{L}}_2\left(\bar{W}_0,\bar{W}_{7/2}\right)-\bar{\tau}\vartheta_1\beta^2\tilde{\mathcal{L}}_2\left(\bar{W}_{1/2},\bar{W}_3\right)-\bar{\tau}\vartheta_1\beta^2\tilde{\mathcal{L}}_2\left(\bar{W}_1,\bar{W}_{5/2}\right)\\ \quad-\bar{\tau}\vartheta_1\beta^2\tilde{\mathcal{L}}_2\left(\bar{W}_{3/2},\bar{W}_2\right)+\bar{\tau}\vartheta_2\tilde{\mathcal{L}}_3(\bar{W}_0,\bar{W}_{7/2})+\bar{\tau}\vartheta_2\tilde{\mathcal{L}}_3(\bar{W}_{1/2},\bar{W}_3)+\bar{\tau}\vartheta_2\tilde{\mathcal{L}}_3(\bar{W}_1,\bar{W}_{5/2})\\ \quad+\bar{\tau}\vartheta_2\tilde{\mathcal{L}}_3(\bar{W}_{3/2},\bar{W}_2)+\dfrac{\bar{\tau}\vartheta_3\beta^2}{2}\tilde{\mathcal{L}}_4\left(\bar{W}_0,\bar{W}_{7/2}\right)+\dfrac{\bar{\tau}\vartheta_3\beta^2}{2}\tilde{\mathcal{L}}_4\left(\bar{W}_{1/2},\bar{W}_3\right)+\dfrac{\bar{\tau}\vartheta_3\beta^2}{2}\tilde{\mathcal{L}}_4\left(\bar{W}_1,\bar{W}_{5/2}\right)\\ \quad+\dfrac{\bar{\tau}\vartheta_3\beta^2}{2}\tilde{\mathcal{L}}_4\left(\bar{W}_{3/2},\bar{W}_2\right)\end{cases}$$

$$O(\epsilon^4):\begin{cases}\mathcal{L}_{11}(\bar{W}_2)+2\bar{\tau}\mathcal{L}_{12}(\bar{W}_2)-\dfrac{\partial^2\bar{F}_4}{\partial X^2}=\beta^2\tilde{\mathcal{L}}_1(\bar{W}_0,\bar{F}_4)+\beta^2\tilde{\mathcal{L}}_1\left(\bar{W}_{1/2},\bar{F}_{7/2}\right)+\beta^2\tilde{\mathcal{L}}_1(\bar{W}_1,\bar{F}_3)\\ \quad+\beta^2\tilde{\mathcal{L}}_1\left(\bar{W}_{3/2},\bar{F}_{5/2}\right)+\beta^2\tilde{\mathcal{L}}_1(\bar{W}_2,\bar{F}_2)+\beta^2\tilde{\mathcal{L}}_1\left(\bar{W}_{5/2},\bar{F}_{3/2}\right)+\beta^2\tilde{\mathcal{L}}_1(\bar{W}_3,\bar{F}_1)\\ \quad+\beta^2\tilde{\mathcal{L}}_1\left(\bar{W}_{7/2},\bar{F}_{1/2}\right)+\beta^2\tilde{\mathcal{L}}_1(\bar{W}_4,\bar{F}_0)+Q_4\\ \mathcal{L}_{21}(\bar{F}_4)+2\bar{\tau}\mathcal{L}_{22}(\bar{W}_4)+\dfrac{\partial^2\bar{W}_4}{\partial X^2}=-\dfrac{\beta^2}{2}\tilde{\mathcal{L}}_1(\bar{W}_0,\bar{W}_4)-\dfrac{\beta^2}{2}\tilde{\mathcal{L}}_1\left(\bar{W}_{1/2},\bar{W}_{7/2}\right)-\dfrac{\beta^2}{2}\tilde{\mathcal{L}}_1(\bar{W}_1,\bar{W}_3)\\ \quad-\dfrac{\beta^2}{2}\tilde{\mathcal{L}}_1\left(\bar{W}_{3/2},\bar{W}_{5/2}\right)-\dfrac{\beta^2}{2}\tilde{\mathcal{L}}_1(\bar{W}_2,\bar{W}_2)-\bar{\tau}\vartheta_1\beta^2\tilde{\mathcal{L}}_2(\bar{W}_0,\bar{W}_4)-\bar{\tau}\vartheta_1\beta^2\tilde{\mathcal{L}}_2\left(\bar{W}_{1/2},\bar{W}_{7/2}\right)\\ \quad-\bar{\tau}\vartheta_1\beta^2\tilde{\mathcal{L}}_2(\bar{W}_1,\bar{W}_3)-\bar{\tau}\vartheta_1\beta^2\tilde{\mathcal{L}}_2\left(\bar{W}_{3/2},\bar{W}_{5/2}\right)-\bar{\tau}\vartheta_1\beta^2\tilde{\mathcal{L}}_2(\bar{W}_2,\bar{W}_2)+\bar{\tau}\vartheta_2\tilde{\mathcal{L}}_3(\bar{W}_0,\bar{W}_4)\\ \quad+\bar{\tau}\vartheta_2\tilde{\mathcal{L}}_3(\bar{W}_{1/2},\bar{W}_{7/2})+\bar{\tau}\vartheta_2\tilde{\mathcal{L}}_3(\bar{W}_1,\bar{W}_3)+\bar{\tau}\vartheta_2\tilde{\mathcal{L}}_3(\bar{W}_{3/2},\bar{W}_{5/2})+\bar{\tau}\vartheta_2\tilde{\mathcal{L}}_3(\bar{W}_2,\bar{W}_2)\\ \quad+\dfrac{\bar{\tau}\vartheta_3\beta^2}{2}\tilde{\mathcal{L}}_4(\bar{W}_0,\bar{W}_4)+\dfrac{\bar{\tau}\vartheta_3\beta^2}{2}\tilde{\mathcal{L}}_4\left(\bar{W}_{1/2},\bar{W}_{7/2}\right)+\dfrac{\bar{\tau}\vartheta_3\beta^2}{2}\tilde{\mathcal{L}}_4(\bar{W}_1,\bar{W}_3)\\ \quad+\dfrac{\bar{\tau}\vartheta_3\beta^2}{2}\tilde{\mathcal{L}}_4\left(\bar{W}_{3/2},\bar{W}_{5/2}\right)+\dfrac{\bar{\tau}\vartheta_3\beta^2}{2}\tilde{\mathcal{L}}_4(\bar{W}_2,\bar{W}_2)\end{cases}\tag{A1}$$

The sets of perturbation equations for the boundary layer solutions are:

$$O(\epsilon^{5/2}):\begin{cases}\vartheta_4\dfrac{\partial^4\widetilde{W}_{3/2}}{\partial\xi^4}-\dfrac{\partial^2\tilde{F}_{5/2}}{\partial\xi^2}=0\\ \vartheta_1\dfrac{\partial^4\tilde{F}_{5/2}}{\partial\xi^4}+(1-2\bar{\tau}\vartheta_1)\dfrac{\partial^2\widetilde{W}_{3/2}}{\partial\xi^2}=0\end{cases}$$

$$O(\epsilon^{3}):\begin{cases}\vartheta_4\dfrac{\partial^4\widetilde{W}_{2}}{\partial\xi^4}-\dfrac{\partial^2\tilde{F}_{3}}{\partial\xi^2}=0\\ \vartheta_1\dfrac{\partial^4\tilde{F}_{3}}{\partial\xi^4}+(1-2\bar{\tau}\vartheta_1)\dfrac{\partial^2\widetilde{W}_{2}}{\partial\xi^2}=0\end{cases}$$

$$O(\epsilon^{5/2}):\begin{cases}\vartheta_4\dfrac{\partial^4\widehat{W}_{3/2}}{\partial\varsigma^4}-\dfrac{\partial^2\hat{F}_{5/2}}{\partial\varsigma^2}=0\\ \vartheta_1\dfrac{\partial^4\hat{F}_{5/2}}{\partial\varsigma^4}+(1-2\bar{\tau}\vartheta_1)\dfrac{\partial^2\widehat{W}_{3/2}}{\partial\varsigma^2}=0\end{cases}$$

$$O(\epsilon^{3}):\begin{cases}\vartheta_4\dfrac{\partial^4\widehat{W}_{2}}{\partial\varsigma^4}-\dfrac{\partial^2\hat{F}_{3}}{\partial\varsigma^2}=0\\ \vartheta_1\dfrac{\partial^4\hat{F}_{3}}{\partial\varsigma^4}+(1-2\bar{\tau}\vartheta_1)\dfrac{\partial^2\widehat{W}_{2}}{\partial\varsigma^2}=0\end{cases}\tag{A2}$$

The obtained asymptotic solution corresponding to clamped edge supports are:

$$W=\mathcal{A}_{00}^{(0)}+\epsilon^{3/2}\left[\mathcal{A}_{00}^{(3/2)}-\mathcal{A}_{00}^{(3/2)}\left(\sin\left(\frac{\alpha X}{\sqrt{\epsilon}}\right)+\cos\left(\frac{\alpha X}{\sqrt{\epsilon}}\right)\right)e^{-\frac{\alpha X}{\sqrt{\epsilon}}}-\mathcal{A}_{00}^{(3/2)}\left(\sin\left(\frac{\alpha(\pi-X)}{\sqrt{\epsilon}}\right)+\right.\right.$$
$$\left.\left.\cos\left(\frac{\alpha(\pi-X)}{\sqrt{\epsilon}}\right)\right)e^{-\frac{\alpha(\pi-X)}{\sqrt{\epsilon}}}\right]+\epsilon^2\left[\mathcal{A}_{00}^{(2)}+\mathcal{A}_{11}^{(2)}\sin(mX)\sin(nY)-\mathcal{A}_{00}^{(2)}\left(\sin\left(\frac{\alpha X}{\sqrt{\epsilon}}\right)+\cos\left(\frac{\alpha X}{\sqrt{\epsilon}}\right)\right)e^{-\frac{\alpha X}{\sqrt{\epsilon}}}-\right.$$
$$\left.\mathcal{A}_{00}^{(2)}\left(\sin\left(\frac{\alpha(\pi-X)}{\sqrt{\epsilon}}\right)+\cos\left(\frac{\alpha(\pi-X)}{\sqrt{\epsilon}}\right)\right)e^{-\frac{\alpha(\pi-X)}{\sqrt{\epsilon}}}\right]+\epsilon^4\left[\mathcal{A}_{00}^{(4)}+\mathcal{A}_{11}^{(4)}\sin(mX)\sin(nY)+\mathcal{A}_{20}^{(4)}\cos(2mX)+\right.$$
$$\left.\mathcal{A}_{02}^{(4)}\cos(2nY)+\mathcal{A}_{22}^{(4)}\cos(2mX)\cos(2nY)\right]+O(\epsilon^5)\tag{A3}$$

$$F=-\mathcal{B}_{00}^{(0)}\left(\beta^2X^2+\wp\frac{Y^2}{2}\right)+\epsilon^2\left[-\mathcal{B}_{00}^{(2)}\left(\beta^2X^2+\wp\frac{Y^2}{2}\right)+\mathcal{B}_{11}^{(2)}\sin(mX)\sin(nY)\right]+$$
$$\epsilon^{5/2}\left[+\mathcal{A}_{00}^{(3/2)}\left(\mathcal{b}_{10}^{(3/2)}\sin\left(\frac{\alpha X}{\sqrt{\epsilon}}\right)+\mathcal{b}_{01}^{(3/2)}\cos\left(\frac{\alpha X}{\sqrt{\epsilon}}\right)\right)e^{-\frac{\alpha X}{\sqrt{\epsilon}}}+\mathcal{A}_{00}^{(3/2)}\left(\mathcal{b}_{10}^{(5/2)}\sin\left(\frac{\alpha(\pi-X)}{\sqrt{\epsilon}}\right)+\right.\right.$$
$$\left.\left.\mathcal{b}_{01}^{(5/2)}\cos\left(\frac{\alpha(\pi-X)}{\sqrt{\epsilon}}\right)\right)e^{-\frac{\alpha(\pi-X)}{\sqrt{\epsilon}}}\right]+\epsilon^3\left[\mathcal{A}_{00}^{(2)}\left(\mathcal{b}_{10}^{(3)}\sin\left(\frac{\alpha X}{\sqrt{\epsilon}}\right)+\mathcal{b}_{01}^{(3)}\cos\left(\frac{\alpha X}{\sqrt{\epsilon}}\right)\right)e^{-\frac{\alpha X}{\sqrt{\epsilon}}}+\right.$$
$$\left.\mathcal{A}_{00}^{(2)}\left(\mathcal{b}_{10}^{(3)}\sin\left(\frac{\alpha(\pi-X)}{\sqrt{\epsilon}}\right)+\mathcal{b}_{01}^{(3)}\cos\left(\frac{\alpha(\pi-X)}{\sqrt{\epsilon}}\right)\right)e^{-\frac{\alpha(\pi-X)}{\sqrt{\epsilon}}}\right]+\epsilon^4\left[-\mathcal{B}_{00}^{(4)}\left(\beta^2X^2+\wp\frac{Y^2}{2}\right)+\mathcal{B}_{20}^{(4)}\cos(2mX)+\right.$$
$$\left.\mathcal{B}_{02}^{(4)}\cos(2mY)+\mathcal{B}_{22}^{(4)}\cos(2mX)\cos(2nY)\right]+O(\epsilon^5)\tag{A4}$$

in which

$$\alpha = \sqrt{\frac{a}{2}} \quad , \quad a = \sqrt{\frac{1-2\bar{\tau}\vartheta_1}{\vartheta_1\vartheta_4}}$$

The periodicity condition yields

$$\mathcal{A}_{00}^{(0)} = 0 \tag{A5}$$

$$\mathcal{A}_{00}^{(3/2)} = \frac{2}{3}3^{1/4}\mathcal{P}_q\left(\frac{2\vartheta_1 - \vartheta_2\mathcal{p}}{1-2\bar{\tau}\vartheta_1}\right) + \left(\frac{2\bar{\tau}\vartheta_6(\vartheta_1-\vartheta_2)}{1-2\bar{\tau}\vartheta_1}\right)\epsilon^{-1/2} \tag{A6}$$

$$\mathcal{A}_{00}^{(2)} = 0 \tag{A7}$$

$$\mathcal{A}_{00}^{(4)} = \frac{2\bar{\tau}\vartheta_2 m^2 + \beta^2 n^2(1-2\bar{\tau}\vartheta_1)}{8(1-2\bar{\tau}\vartheta_1)}\left(\mathcal{A}_{11}^{(2)}\right)^2 \tag{A8}$$

The parameters in equations (36-39) are as follow (A9)

$$\mathcal{P}_q^{(0)} = K_0K_1\beta^2 + K_2\beta^2\epsilon^2$$

$$\mathcal{P}_q^{(2)} = 8K_1K_3K_8\beta^2 + \frac{8K_1K_3\beta^2(K_0K_1K_7\beta^2 + K_0K_3K_6)}{K_0K_1\beta^2 - K_6} + \frac{4K_1K_3\beta^2(K_0K_7 + K_0^2K_3)}{K_0K_1\beta^2 - K_6} + 16K_0K_3K_4\beta^2 + \frac{4K_0K_1K_3K_{10}\beta^2}{K_0K_5 + K_9} \tag{A10}$$

$$\delta_q^{(0)} = \left[\frac{3^{3/4}}{2}\bar{\tau}\vartheta_6(\vartheta_1-\vartheta_2)\right]\epsilon^{-1/2} + \left[\frac{2\bar{\tau}^2\vartheta_2(\vartheta_1-\vartheta_2)}{\beta^2(1-2\bar{\tau}\vartheta_1)}\right]\epsilon^{-1} + \left[\frac{\vartheta_1\mathcal{p}}{2} - \vartheta_2 - \bar{\tau}\vartheta_2\left(\frac{2\vartheta_1 - \mathcal{p}\vartheta_2}{1-2\bar{\tau}\vartheta_1}\right) + \left(\frac{2\vartheta_1\vartheta_2 - \mathcal{p}\vartheta_2^2}{\pi\alpha\vartheta_1(1-2\bar{\tau}\vartheta_1)}\right)\epsilon^{1/2}\right]\mathcal{P}_q + \left[\left(\frac{3^{1/4}\alpha(2\vartheta_1 - \mathcal{p}\vartheta_2)^2}{6\pi(1-2\bar{\tau}\vartheta_1)}\right)\epsilon\right]\mathcal{P}_q^2 \tag{A11}$$

$$\delta_q^{(2)} = \left[\frac{3^{3/4}}{32}\left((m^2(1-2\bar{\tau}\vartheta_1) + 2\bar{\tau}\vartheta_2\beta^2n^2) - \frac{4\bar{\tau}^2\vartheta_2^2m^2 + 2\bar{\tau}\vartheta_2\beta^2n^2(1-2\bar{\tau}\vartheta_1)}{1-2\bar{\tau}\vartheta_1}\right)\right]\epsilon^{-3/2} \tag{A12}$$

where $K_i \quad (i = 0, \dots, 10)$ are the parameters in terms of $\vartheta_1, \vartheta_2, \vartheta_3, \vartheta_4, \vartheta_5, m, n, \beta, \mathcal{p}$ obtained via the sets of perturbation equations. (A13)

$$\mathcal{S}_1 = -\left[\left(\frac{2\vartheta_1 - \vartheta_2\mathcal{p}}{1-2\bar{\tau}\vartheta_1}\right)\left(\mathcal{P}_q^{(2)}\right)\right]$$

$$\mathcal{S}_2 = -\left(\frac{2\vartheta_1 - \vartheta_2\mathcal{p}}{1-2\bar{\tau}\vartheta_1}\right)\left(\mathcal{P}_q^{(0)}\right) - \left(\frac{2\bar{\tau}\vartheta_6(\vartheta_1-\vartheta_2)}{1-2\bar{\tau}\vartheta_1}\right)\epsilon \tag{A14}$$